This is a repository copy of *Multi-walled carbon nanotube dispersion methodologies in alkaline media and their influence on mechanical reinforcement of alkali-activated nanocomposites*.

White Rose Research Online URL for this paper:
https://eprints.whiterose.ac.uk/191499/

Version: Accepted Version

Article:
Davoodabadi, M. orcid.org/0000-0002-9868-5575, Liebscher, M., Hampel, S. et al. (6 more authors) (2021) Multi-walled carbon nanotube dispersion methodologies in alkaline media and their influence on mechanical reinforcement of alkali-activated nanocomposites. Composites Part B: Engineering, 209. 108559. ISSN 1359-8368

https://doi.org/10.1016/j.compositesb.2020.108559

Article available under the terms of the CC-BY-NC-ND licence (https://creativecommons.org/licenses/by-nc-nd/4.0/).

Reuse
This article is distributed under the terms of the Creative Commons Attribution-NonCommercial-NoDerivs (CC BY-NC-ND) licence. This licence only allows you to download this work and share it with others as long as you credit the authors, but you can't change the article in any way or use it commercially. More information and the full terms of the licence here: https://creativecommons.org/licenses/

Takedown
If you consider content in White Rose Research Online to be in breach of UK law, please notify us by emailing eprints@whiterose.ac.uk including the URL of the record and the reason for the withdrawal request.

White Rose
university consortium
Universities of Leeds, Sheffield & York

eprints@whiterose.ac.uk
https://eprints.whiterose.ac.uk/

Multi-walled carbon nanotube dispersion methodologies in alkaline media and their influence on mechanical reinforcement of alkali-activated nanocomposites

Maliheh Davoodabadi[a,b,c], Marco Liebscher[b,*], Silke Hampel[c,*], Massimo Sgarzi[d], Ali Bashiri Rezaie[b], Daniel Wolf[c], Gianaurelio Cuniberti[d,*], Viktor Mechtcherine[b], Jian Yang[a,*]

[a] Department of Civil Engineering, School of Naval Architecture, Ocean and Civil Engineering, Shanghai Jiao Tong University, 200240 Shanghai, PR China

[b] Institute of Construction Materials, Faculty of Civil Engineering, TU Dresden, 01062 Dresden, Germany

[c] Leibniz Institute for Solid State and Materials Research, 01069 Dresden, Germany

[d] Institute for Materials Science and Max Bergmann Centre of Biomaterials, TU Dresden, 01062 Dresden, Germany

*Corresponding authors: j.yang.1@sjtu.edu.cn (J.Yang), marco.liebscher@tu-dresden.de (M. Liebscher), S.Hampel@ifw-dresden.de (S.Hample), gianaurelio.cuniberti@tu-dresden.de (G. Cuniberti)

Abstract

The focus of present research is the establishment of a practical procedure for effective incorporation of multi-walled carbon nanotubes (MWCNTs) into alkali-activated materials (AAMs) with the aim of mechanical reinforcement. Investigated composite in this work was an alkali-activated matrix composed of fly ash (FA) and ground-granulated blast furnace-slag (GGBS) as solid aluminium-calcium-silicate precursors along with highly concentrated sodium silicate (Na_2SiO_3) and sodium hydroxide (NaOH) as liquid alkaline activators. Na_2SiO_3, NaOH, and a combination of them were used for dispersion of MWCNTs. An anionic surfactant, naphthalene sulfonate (NS), and ultrasonication were applied to assist in the preparation of nanofluids. Optical microscopy, integral light transmission (ILT), and Fourier-transform infrared spectroscopy (FTIR) were performed to assess the colloidal behaviour of MWCNTs in the nanofluids. The possible dispersion mechanisms were furthermore hypothesized for each alkaline medium. Based on the outcomes, MWCNTs had the best dispersion performance in the Na_2SiO_3 based nanofluids. The relevant nanocomposites, accordingly, in comparison to the other preparation methodologies in this research, indicated the highest

improvements in flexural (65%) and compressive (30%) strengths as a consequence of 0.050 wt.% MWCNT incorporation. Scanning electron microscopy (SEM) and mercury intrusion porosimetry (MIP) further clarified the reinforcement functionality and microstructure refinement of the MWCNTs dispersed in the Na_2SiO_3 based nanofluids. Altogether, this paper represents a broad insight concerning a better understanding of MWCNTs' interactions in alkaline activators, i.e., dispersion media, and AAMs, i.e., host matrices, to obtain the highest possible mechanical and microstructural performance of reinforced nanocomposites.

Keywords

Carbon nanotubes, Alkali-activated materials, Nanofluids, Nanocomposites, Colloidal interactions, Mechanical properties, Microstructure.

1. Introduction

In comparison to cementitious materials, alkali-activated materials (AAMs) and geopolymers are more sustainable with a lower environmental footprint [1]. Their main precursor components can be obtained from industrial by-products and the possibility of being waste-originated has been recently introduced for the activators [2,3]. They can be particularly formulated to exhibit higher mechanical strength, faster hardening, and lower permeability [4]. Moreover, excellent resistance to aggressive conditions, e.g., heat and chemicals, and potential waste encapsulation are increasing the academic favourability of AAMs and geopolymers [5]. However, similar to their cementitious counterparts [6], there is an emerging tendency to the manufacture of reinforced alkali-activated and geopolymeric composites because of the demands for higher mechanical strength, strain capacity, ductility, and durability [7–10]. Therefore, a wide range of fibres with different origins have been utilized to fulfil those demands [11–15].

In parallel, carbon nanotubes (CNTs) have been predominantly implemented in cementitious nanocomposites to reinforce the matrices and modify the structural [16] and non-structural [17] properties of the composites, which is unique considering the diversity of their applications [18]. CNTs are able to provide an inclusive package of multifunctional characteristics with competitively rather lower quantities than other common nanofillers [19]. Thus, their application in alkali-activated materials (AAMs) is very desirable [20]. Nevertheless, it appears that to date, the incorporation of CNTs into AAMs has been put into the practice to a far less extent [21].

Regarding the fact that AAMs first introduced with a two-part concept, i.e., non-aqueous design, availability of water, a low ionic strength and non-viscous dispersion medium, in the cementitious mix design could be one of the reasons [22]. In a two-part alkali-activated system, viscous bases with extremely high pH and ionic strength are utilized to initiate the leaching of aluminosilicates and polycondensation processes [23]. In the design of two-part AAMs, water should be largely eliminated due to its documented adverse impacts [24]; notwithstanding that fact, water is still included in the design of some two-part AAMs and geopolymers. In such cases, researchers with following cementitious approaches [25], introduced CNTs into the aqueous media but the activation initiated by liquid alkaline activators [26–30]. With the non-aqueous formulation, there is one case reporting CNTs' incorporation with an alkaline dispersion procedure in a two-part composite [31]. Apart from nano matters, mainly hazards arising from utilizing highly alkaline, viscous and corrosive liquids, has recently put a one-part approach forward to overcome practical difficulties which will additionally facilitate nanoinclusions [32–34].

This predilection of researchers to disperse CNTs in water, despite adopting two-part approach, may stem from the unclear interactions among CNTs, surfactant, and alkaline media. Some studies have assessed the behaviour of CNTs in high-pH liquid environments, but other important alkaline properties, i.e., high solid concentration, ionic strength, viscosity, and density, have scarcely been evaluated. Because simulation of the alkaline environments was attempted either by introducing a diluted base of very low molarity into the water or by reversely diluting alkaline media to lower concentrations using water. These procedures are far away from real liquid alkaline conditions. For example, one view showed higher dispersibility of MWCNTs in alkaline pH solutions [35], but in contrast, other researchers concluded that CNT suspensions will not maintain the stability in highly alkaline media [36]; or a medium with neutral pH can be an optimum environment for MWCNT dispersion [37]. Simulation of MWCNT exposure to diluted sodium silicate furthermore confirmed the agglomeration and instability of CNTs in such environments [38]. Therefore, the dispersion of CNTs into alkaline media while maintaining all their basic characteristics is a crucial and interesting challenge, which is not comprehensively investigated in the literature so far. Furthermore, that dispersion status of CNTs can have a significant influence on the nanocomposite's mechanical, structural, and microstructural properties. Likewise, this issue has not been thoroughly

studied in the literature, and to date the potential mechanisms and interactions for AAMs are not well understood and described.

Considering all these grounds, in the present paper it is aimed to study the fabrication concepts and fundamentals of alkali-activated MWCNT nanocomposites. The behaviour of MWCNTs after exposure to both alkaline media and alkali-activated matrix is tried to be elaborated to a feasible extent. Beyond the gaps, mentioned above, the functionality of alkaline-dispersed MWCNTs in blend AAM systems has not been investigated in the literature so far. Hence, finding a successful integration methodology for MWCNTs and AAMs through a highly concentrated and viscous alkaline medium in the framework of a non-aqueous formulation is the significance, novelty, and scientific contribution of this research. To the best of the authors' knowledge, this is one of the first examples in the literature investigating MWCNTs dispersion in different alkaline environments, the effect of surfactant, mechanical features, and the microstructural properties of the ultimate respective nanocomposites.

For this purpose, a blend FA-GGBS alkali-activated composite activated by concentrated Na_2SiO_3 and NaOH has been considered as the host matrix for MWCNTs. The alkali-activated composite is an ambient-cured material rich in silicon, aluminium, calcium, and sodium. Colloidal interactions have been assessed after dispersing MWCNTs into the liquid alkaline activators, i.e., Na_2SiO_3, NaOH and their combination, with the assistance of naphthalene sulfonate and ultrasonication. Possible dispersion mechanisms have been hypothesised for those distinct alkaline media. Attempts have been made to understand whether the colloidal behaviour of nanofluids can be attributed to the mechanical and microstructural performance of nanocomposites.

2. Materials and methods

2.1. Materials

MWCNTs were supplied from SWeNT, USA, under the commercial name of SMW210. The MWCNTs, with inner and outer diameters of 4.5 and 10 nm, were of pristine grade, non-functionalised and non-purified; their main properties are listed in Table 1. The anionic surfactant was the commercially available superplasticizer, MasterRheobuild 30 (BASF, Germany), based on sodium ß-naphthalene sulfonic acid formaldehyde. The naphthalene sulfonate was added as surfactant/dispersant for MWCNT dispersion purposes not for rheology and strength modifications, due to its stability and

functionality in alkali-activated materials in addition to its dispersion capabilities [35,36,47,39–46].

Table 1: MWCNTs morphology and structure provided by SWeNT, USA.

Tube length	wall number	Bulk density	Aspect ratio	Specific surface area	Purity
3 μm	7	0.07 $g.cm^{-3}$	300	350 $m^2.g^{-1}$	84 wt.%

The solid precursors were fly ash (Steament® H-4 FA from Steag Power Minerals GmbH, Germany) and GGBS from Opterra GmbH, Germany. The chemical compositions and physical properties of the solid precursors are listed in Table 2 and Table 3. The solid components were activated by extra-pure sodium silicate (3.5 molar ratio) produced by Merck KGaA, Germany, and sodium hydroxide (dissolved and diluted to 8 molar) by Grüssing GmbH, Germany.

Table 2: EDX analysis of precursors, chemical composition in weight percentage [48].

Constituent	SiO_2	Al_2O_3	CaO	Fe_2O_3	K_2O	MgO	SO_3	TiO_2	Na_2O	MnO
FA (wt.%)	49.30	29.90	1.90	7.70	5.10	-	-	1.40	-	-
GGBS (wt.%)	33.56	8.44	47.49	-	-	4.74	4.14	0.90	0.37	0.37

Table 3: Physical properties of solid precursors [48].

Property	Loss of ignition	Amorphous phase (%)	Crystalline phase (%)	Average particle size D_{50} (μm)
FA	1.51	75.50	24.50	14.80
GGBS	1.35	100.00	-	11.89

2.2. Methods

2.2.1. MWCNTs and surfactant concentrations

MWCNTs' quantity in nanofluids and nanocomposites was considered to be as low as 0.050 wt.% of solid precursors, i.e., FA and GGBS total mass equal to 69 g, which play the most important binding and strength gain role in the main composite. Therefore, MWCNTs' concentration in nanofluids and nanocomposites was the same, i.e., 0.0350 g [21,25-27,49–55]. The concentration of naphthalene sulfonate was considered to be 7% and added with a mass twice as CNTs' mass, based on the preliminary studies.

2.2.2. Fabrication methodologies of nanofluids and nanocomposites

Nanofluids and nanocomposites were synthesized based on three distinct methodologies. The schematic illustration of the preparation steps and components used in each step for all nanofluids, composites, and nanocomposites can be seen in Figure 1 and Table 4. Synthesis methodologies are as followings:

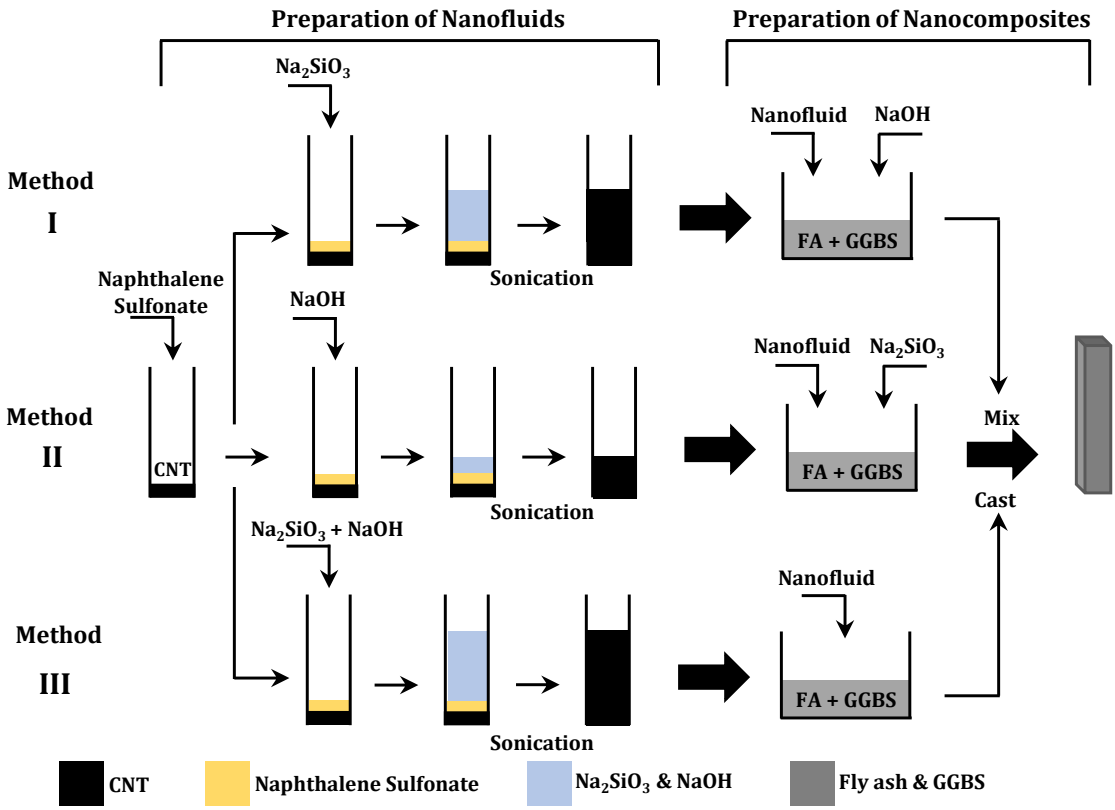

Figure 1: Nanofluids and nanocomposites preparation methodologies. In the figure, black stands for MWCNT, yellow for naphthalene sulfonate, blue for sodium silicate, sodium hydroxide and their combination, and grey for fly ash, GGBS, and the nanocomposite.

I. Na_2SiO_3 based nanofluids and nanocomposites

The nanofluids were produced by adding up MWCNTs, NS dilution, and Na_2SiO_3 and sonicating these solutions. The corresponding nanocomposites were synthesised by mixing FA+GGBS and nanofluids at first, and after 30 seconds, NaOH was mixed with the paste blend. Hence, the liquids (CNTs+NS+Na_2SiO_3 nanofluids, and NaOH) were not in contact beforehand. Relevant references without MWCNTs were prepared in the same manner, surfactant included and excluded.

II. NaOH based nanofluids and nanocomposites

The nanofluids of method II were prepared by sonicating MWCNTs in NS and NaOH. Then the nanofluids were mixed with precursors and the other activator, Na_2SiO_3 to yield the nanocomposites. Reference composites without MWCNTs were prepared similarly with and without NS.

III. Combined (Na_2SiO_3+NaOH) nanofluids and nanocomposites

The nanofluids were produced by dispersing MWCNTs in a pre-combined solution of Na_2SiO_3 and NaOH and the relevant nanocomposite and reference composites were prepared similar to

methodologies I and II.

Table 4: Component proportions used for preparation of all investigated nanofluids, composites and nanocomposites considering proposed methodologies. In the table, black stands for MWCNT, yellow for naphthalene sulfonate, blue for sodium silicate, sodium hydroxide and their combination, and grey for both fly ash and GGBS.

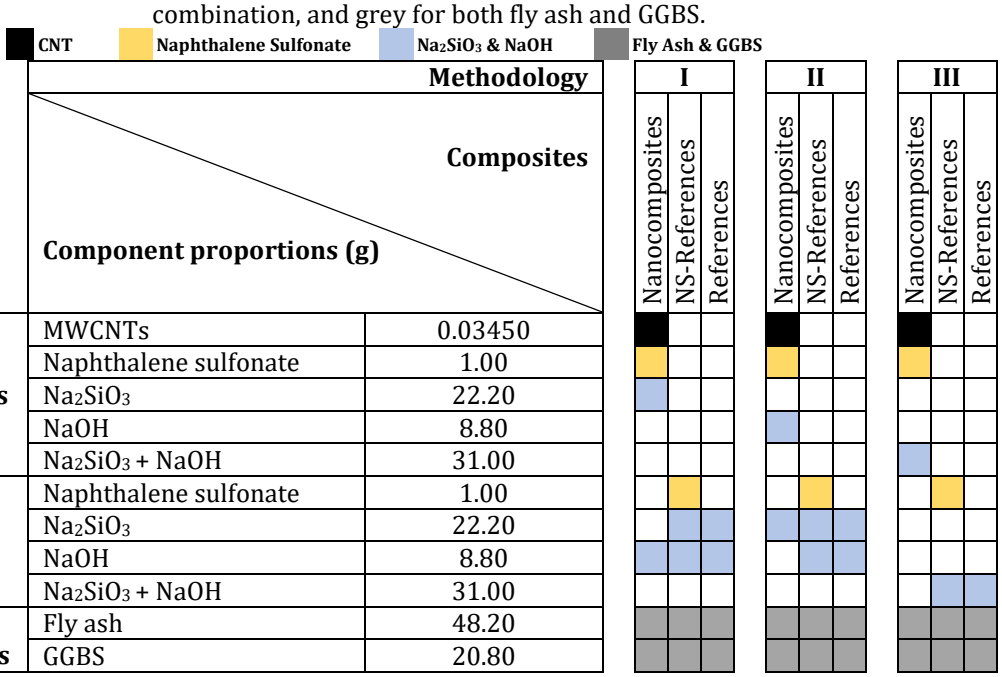

	Component proportions (g)	Methodology I: Nanocomposites	Methodology I: NS-References	Methodology I: References	Methodology II: Nanocomposites	Methodology II: NS-References	Methodology II: References	Methodology III: Nanocomposites	Methodology III: NS-References	Methodology III: References
Nanofluids	MWCNTs: 0.03450	■			■			■		
	Naphthalene sulfonate: 1.00	■			■			■		
	Na_2SiO_3: 22.20	■								
	NaOH: 8.80				■					
	Na_2SiO_3 + NaOH: 31.00							■		
Liquid alkaline activators	Naphthalene sulfonate: 1.00		■			■			■	
	Na_2SiO_3: 22.20		■	■	■	■	■			
	NaOH: 8.80	■	■	■		■	■			
	Na_2SiO_3 + NaOH: 31.00								■	■
Solid precursors	Fly ash: 48.20	■	■	■	■	■	■	■	■	■
	GGBS: 20.80	■	■	■	■	■	■	■	■	■

2.2.3. Dispersion of nanofluids

Nanofluids were dispersed by an ultrasonic homogeniser Sonopuls HD 2070, Bandelin. The probe type was a 2-mm-diameter MS 72 with 285 µm amplitude. Ultrasonication was conducted for two short periods of 5 minutes with 70% of maximum amplitude of the instrument to reach the dispersion plateau [56].

2.2.4. Mixing of nanocomposites

In detail, nanocomposites were fabricated by shear mixing of solid precursors, nanofluids and liquid alkaline activators using an IKA Eurostar 200 control P4. First, dry FA and GGBS were mixed for 3 min at 90 rpm. Next, precursors were stirred with the relevant nanofluids and corresponding liquid alkaline activators, if applicable, for 5 min at 110 rpm. Finally, the obtained pastes were cast in 10×10×60 mm^3 rectangular prismatic moulds. Afterwards the specimens were covered with films of low-density polyethylene (LD-PE) for 20 hours. At last, specimens were demoulded and cured in LD-PE bags for 3 and 28 days at the ambient laboratory environment.

2.2.5. Characterisation of nanofluids

Optical microscopy

Qualitative assessment of fresh nanofluids was carried out using a Keyence digital microscope VHX-6000 in addition to visual observations. To do this a drop of nanofluid was inserted between two microscope slides attached by a 75 μm spacer.

Integral light transmission (ILT)

A dispersion analyser, LUMISizer®, LUM GmbH, Germany, was applied to quantify the dispersion stability of diverse nanofluids in addition to the dispersibility of MWCNTs in alkaline media. The specimens were illuminated by near-infrared light, and transmission throughout the cells was detected by CCD sensors [57]. For this purpose, polycarbonate cuvette cells were filled up to 0.3 mL of nanofluids and illuminated at 22°C temperature and 4000 rpm centrifugation.

Fourier-transform infrared spectroscopy (FTIR)

The FTIR analysis was performed using Bruker Vertex80v spectrometer, Germany, equipped by MCT detector, Hyperion Microscope 2000. The resolution was 2 cm^{-1} in the wavenumber range from 400 to 4000 cm^{-1} at room temperature. A drop of each nanofluid was dried on a KBr crystal substrate.

2.2.6. Characterisation of nanocomposites

Mechanical experiments

Three-point-bending and compression tests were performed using a Zwick 1445 universal testing system, Germany, at 1 $mm.min^{-1}$ displacement control and force capacity of 1 kN for bending and 10 kN for compression at ages of 3 and 28 days. For the analytical experiments following mechanical tests, specimens were immersed in isopropanol for pore solution exchange and afterwards, dried in laboratory standard conditions. This can slow down chemical reactions without deteriorating the matrix microstructure [58].

Scanning electron microscopy (SEM)

Fractured surfaces were imaged by FEI Quanta™ 250 FEG-ESEM in high vacuum conditions at an age of 28 days. Moreover, chemical composition of precursors was obtained by this FEG-ESEM.

Mercury intrusion porosimetry (MIP)

Microstructure was analysed by means of a Porotec Mercury Porosimeter PASCAL 140 under 300 kPa pressure and a PASCAL 440 with a pressure range from 0 to 400 MPa for detection of ultra-fine pores in 28-day specimens.

3. Results and discussion

3.1. Nanofluids' performance characterisation

3.1.1. MWCNTs dispersiblity and de-agglomeration

To assess the behaviour of MWCNTs in alkaline media, first the MWCNTs were dispersed in Na_2SiO_3, NaOH, and compound media without surfactant (i.e., naphthalene sulfonate); see Figure 2(a). In the fresh state, MWCNTs stay on the surface of NaOH and combined suspensions; however, in Na_2SiO_3, they start to settle down immediately after adding Na_2SiO_3. This settling is an important factor in demonstrating the amount of dispersible MWCNTs and can be attributed to the chemical composition and physical properties of Na_2SiO_3. After ultrasonication, a large quantity of MWCNTs were dispersed in Na_2SiO_3; see Figure 2(a). All nanofluids seem black and semi-dark; nonetheless Na_2SiO_3 nanofluid is very opaque and well dispersed, while NaOH and compound nanofluids are rather transparent. This fact is not evident in Figure 2; instead, the presence of bulky agglomerates can be easily seen on the surface of NaOH and compound nanofluids. The colloidal behaviour of MWCNTs when dispersed in Na_2SiO_3 without NS is unique. The nanofluid is a viscous gel whose agglomerates are in swollen state although of much smaller size than in the other alkaline media, as can be seen in the optical micrographs in Figure 3(a, c, e).

Media effects can be further investigated when naphthalene sulfonate is included into the nanofluids. The viscosity of Na_2SiO_3 as compared to NaOH reduce the mobility of MWCNTs, which is obvious in the fresh state of Na_2SiO_3 and compound nanofluids; see Figure 2(b). In compound nanofluids, MWCNTs form the settled agglomerated layer faster than in Na_2SiO_3, and in NaOH even much faster because of the differences already mentioned. With naphthalene sulfonate addition, MWCNTs are dispersible in all alkaline media: after ultrasonication, nanofluids are very dark and rather opaque. MWCNTs have a considerable specific surface area (350 m^2g^{-1}, see Table 1), which make them suitable for the adsorption of surfactant molecules. Because of the repulsive forces acting among the adsorbed surfactant and the imposed energy of sonication, new adsorption sites are created on the nanotube surface, resulting in the progressive dispersion of single MWCNTs [59]. This dimension reduction occurred in all nanofluids, with the smallest size observed for MWCNTs in Na_2SiO_3 nanofluids and largest in compound nanofluids, as seen in the optical micrographs in Figure 3(b, d, f).

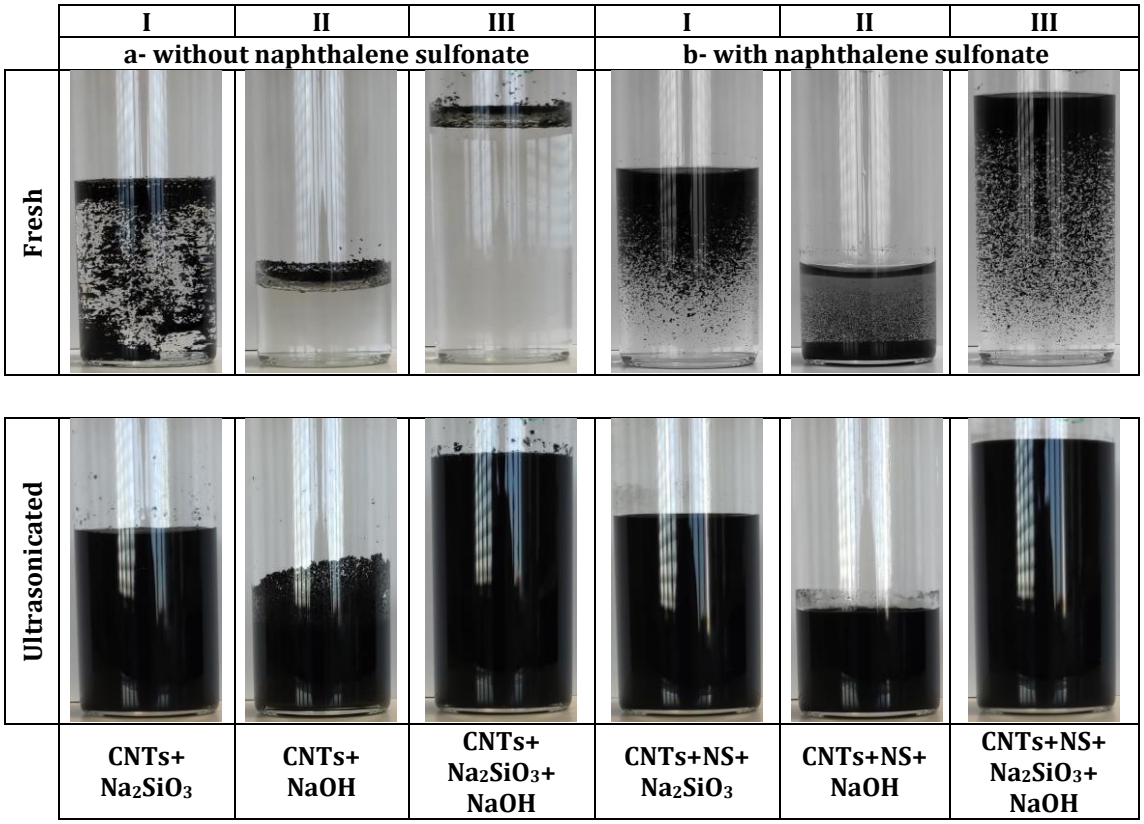

Figure 2: Dispersion of MWCNTs in alkaline media; MWCNTs conc. 0.050 wt.% of precursors.

3.1.2. MWCNTs dispersion stability

Integral light transmission measurements quantify the dispersibility and stability of nanofluids, which is in parallel a way of agglomeration and settlement analysis of MWCNTs within each nanofluid. Generally, a lower percentage of light transmission and a smaller gradient of graphs represent better dispersibility and higher stability of MWCNTs, respectively. Duration period is an optional parameter, and experiments are conducted under centrifuge circumstances. Therefore, duration can be extended to hours and revolution can be set to the maximum to simulate real conditions for MWCNTs as much as possible, from nanofluid preparation until destination in the matrix. That can be theoretically hypothesised as both short-term in-solution and long-term in-matrix behaviour of MWCNTs, i.e., aging phenomenon. Available centrifugal and gravitational forces can be supposed as pressures to be encountered by MWCNTs after exposure to the semi-solid matrix. The investigated alkali-activated matrix is completely hardened within a few hours, as observed during nanocomposite preparations. Based on that ground, ILT measurements were extended up to 5 hours for the hypothesised purposes mentioned.

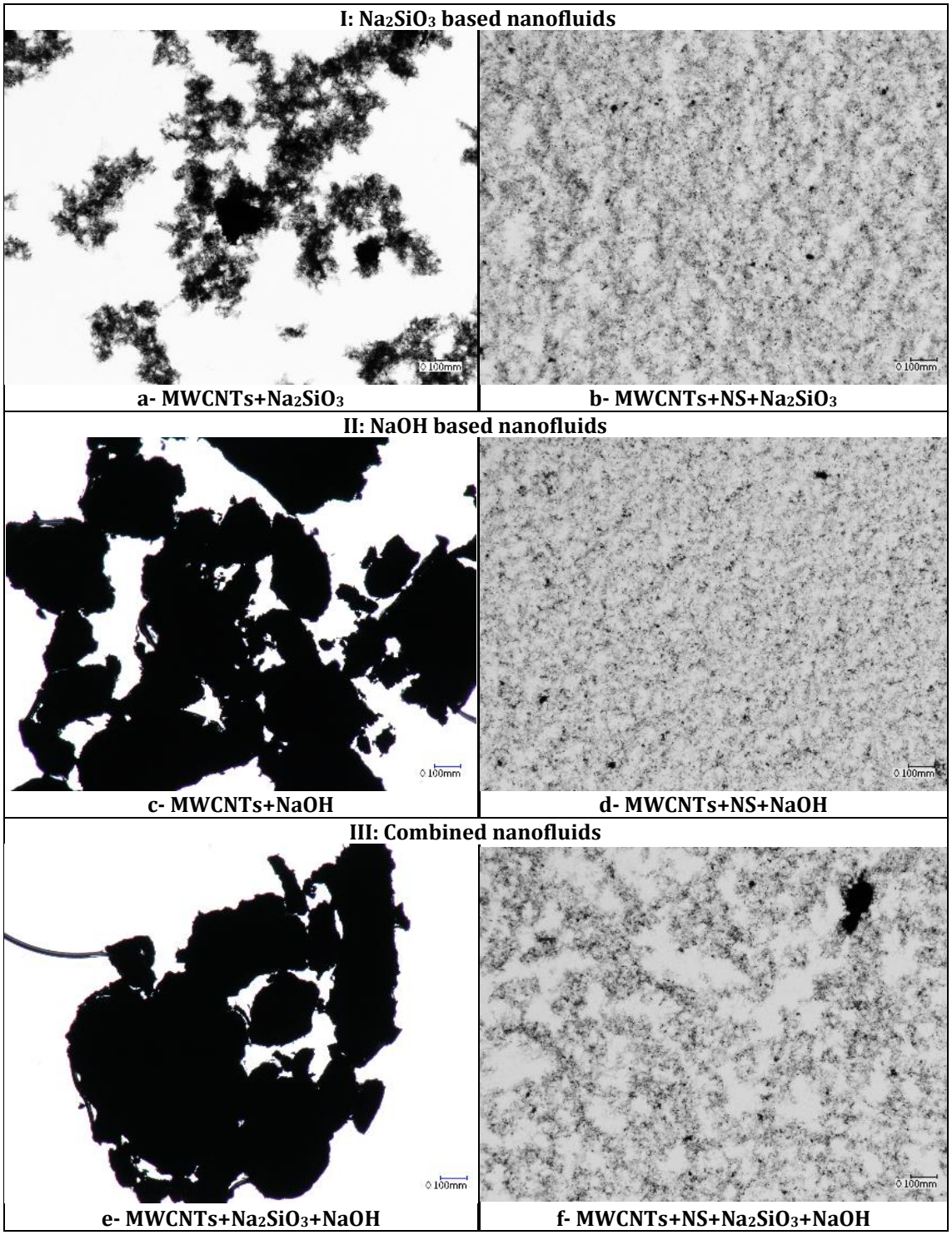

Figure 3: Optical micrographs of MWCNTs dispersed in alkaline media.

According to ILT measurement results presented in Figure 4(a), MWCNTs in Na_2SiO_3 nanofluids without surfactant show initial light transmission of 4%, meaning very opaque and containing a considerable quantity of MWCNTs, i.e., excellent dispersibility. Final transmission of the nanofluid reaches approximately 30% as shown by a horizontal curve, which is a proof of its being

rather stable over time. MWCNTs in NaOH and compound nanosuspensions have almost 25% and 80% initial light transmission, which is a sign of non-dispersibility. These nanofluids are not stable and settle rapidly, letting a large proportion of light pass through the specimens during ILT measurements.

Inclusion of naphthalene sulfonate causes a slight improvement in dispersibility of MWCNTs in Na_2SiO_3, as reflected in initial transmission of 3% compared to 4% without surfactant; see Figure 4(b). With a final transmission of more than 50%, Na_2SiO_3 nanofluid is less stable than nanofluid without naphthalene sulfonate over the long term. Thus, the main function of NS in Na_2SiO_3 is triggering single MWCNTs dispersion, and the dispersibility-stability of MWCNTs is determined more by the physicochemical properties of Na_2SiO_3, as explained above for Figure 3(a, b). With naphthalene sulfonate inclusion, a size reduction of the largest agglomerates can be observed for all nanofluids. The presence of naphthalene sulfonate in NaOH and compound nanofluids furthermore contributes strongly to the dispersibility of MWCNTs. The comparison of Figure 4(a, b) illustrates the reduction of integral transmission for these nanofluids from 25% for compound and 80% for NaOH to 3% for both.

Considering the ILT results in Figure 4(b), MWCNTs in alkaline media display three distinguished behaviours. At first, MWCNTs experience a period of in-solution stability, which is very long for Na_2SiO_3 nanofluid, while it is very short for NaOH nanofluid. Afterwards, MWCNTs display transient behaviour, where they abruptly settle down in NaOH nanofluid, while they sediment at a lower rate in the two other media. Lastly, MWCNTs demonstrate both agglomeration and settlement. This phase can be hypothesized as an approximation of anticipated in-matrix behaviour of MWCNTs after exposure to the matrix as explained above. With this perspective, Na_2SiO_3 based nanofluid is the most stable strategy in both in-solution and anticipated in-matrix circumstances and contains the smallest agglomerate dimensions; see Figure 3(b) and Figure 4(b). Consequently, Na_2SiO_3 can be considered as a very promising host medium for MWCNT dispersion. On the other hand, compound Na_2SiO_3+NaOH based nanofluid demonstrates the most in-matrix unstable behaviour with the largest agglomerates sizes; see Figure 3(f) and Figure 4(b). In the middle, NaOH based nanofluid shows in-solution instability with the highest rate, but the agglomerate dimensions are comparable to Na_2SiO_3 nanofluid; see Figure 3(d) and Figure 4(b).

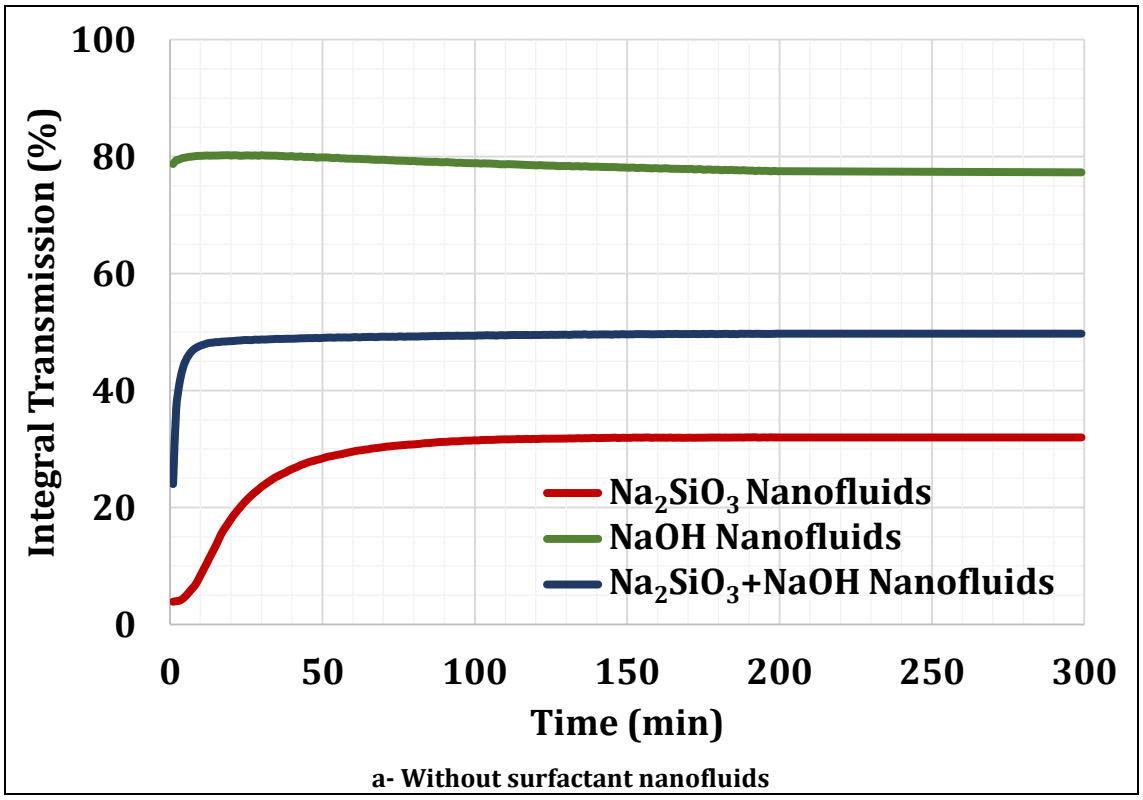

a- Without surfactant nanofluids

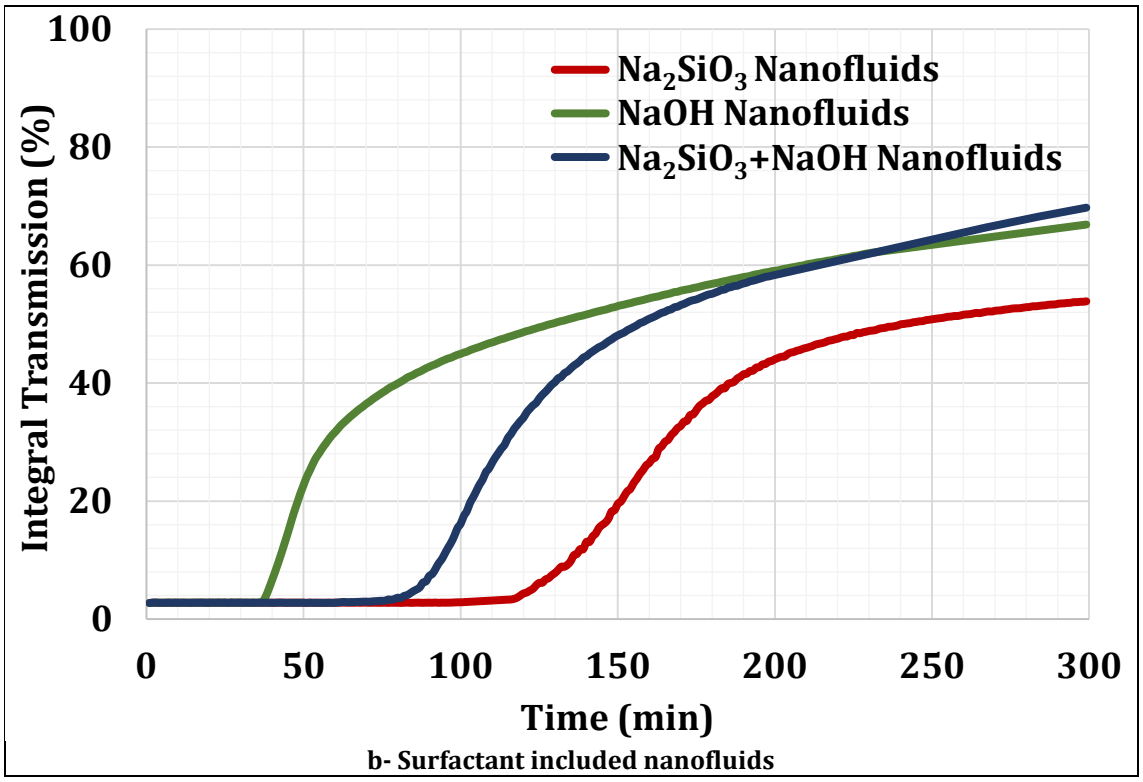

b- Surfactant included nanofluids

287 Figure 4: Dispersibility and stability evaluation of MWCNTs in alkaline media by ILT measurements.

288 It should be considered that even though all nanofluids contain the same quantity of MWCNTs, the

289 concentration changes to a great extent based on the water content of each investigated medium.

NaOH nanofluid has the smallest amount of medium; hence, MWCNT concentration is much higher than in the other nanofluids. This high concentration may affect the dispersion characteristics and the agglomerate dimensions to some extent, but generally observed behaviour and trends, i.e., initial dispersibility and abrupt instability of NaOH nanofluids, may not be significantly affected. It should be considered that in general incorporated MWCNT concentration is just 0.050 wt.% of solid precursors.

3.1.3. MWCNTs and naphthalene sulfonate interactions

MWCNTs can be considered as rolled-up graphene layers with a π-conjugated electron system. They possess extremely high structural stability, hydrophobicity, and specific surface area. These features enable MWCNTs to be an excellent adsorbent considering intermolecular interactions such as π-π stacking [60,61]. Applied herein the surfactant, naphthalene sulfonate, has an aromatic structure as a compatible feature to CNTs. Therefore, it is able to undergo π-π interactions as well [62]. CNTs, even in entanglement, have adequate surfactant adsorption sites, for instance peripheral tube surfaces, exterior and interior intersections, and even intra-tubular sites in the case of open-end tubes [63].

Carbon content, number of aromatic cycles, and degree of graphitisation contribute most to the efficiency of adsorption [64,65]. On the other hand, oxygen-containing impurities, carboxyl or hydroxyl, will reduce the hydrophobicity and weaken the strength of the π-system [66]. Moreover, the number of polar sulfonate heads of surfactant correlate inversely with the adsorption density, even though it may be advantageous for better interaction of surfactant and polar media [67].

Considering the findings of the dispersion analysis (ref. section 3.1.2), physisorption of naphthalene sulfonate on MWCNTs in alkaline media may occur by the π-stacking of the benzene rings of NS on the graphene lattice of MWCNTs. This can be strengthened by the media effect when hydrophilic head of naphthalene sulfonate, i.e., sodium sulfonate, interacts with the polar alkaline solution. These simultaneous re-orientations and interactions happen mostly when the surfactant contains one or more aromatic carbon rings and polar groups in its structure. The mentioned attractions are amongst long-decay ranged van der Waals forces and are quite strong [68,69]. The MWCNT and naphthalene sulfonate interactions discussed are further described by FTIR spectroscopy of three nanofluids under investigation.

FTIR spectroscopy is an analytical technique for the chemical identification of functional groups, e.g., –OH and –COOH [70], by detecting the presence or absence of particular bands in the IR spectra [71]. FTIR is frequently used to study sulfonic-acid-containing surfactants such as sodium dodecylbenzene sulfonate (SDBS) [72], sodium dodecyl sulfate (SDS) [73], melamine sulfonate (MS) [74] and 4, 4′-di (n-tetradecyl) diphenylmethane disulfate salt (DSDM) [75] adsorption on the CNTs in aqueous media. In this paper, FTIR is similarly used to characterise the nanofluids.

FTIR spectra of Na_2SiO_3 based and Na_2SiO_3+NaOH based nanofluids present similar patterns (Figure 5, Table 5) due to the presence of sodium metasilicate [76,77]. The broad band centred at circa 2970 cm^{-1} is ascribable to combination modes and overtones of SiO_3^{2-} species [76–78]. Additionally, CH stretching of the naphthalene ring of NS fall in this spectral region [41,75,79]. The broad band centred at 1830 cm^{-1} and the one in the 1675-1650 cm^{-1} range are attributed to the combination of symmetric and asymmetric stretching of Si-O-Si [77]. The 1150-850 cm^{-1} range comprises the asymmetric and symmetric stretching modes of O-Si-O, and the ring breathing and CH bending of NS [78,79]. The peak in the 780-450 cm^{-1} range is attributed to the skeleton distortion of NS [79], and to stretching and bending modes of O-Si-O [71]. The weak band at 1457 cm^{-1} present in the combination nanofluid is related to NS, and ascribable to CH bending [79] and to -SO_2- asymmetric stretching [80].

On the other hand, NaOH based nanofluid present a different IR spectrum, which presents vibration modes of NS together with the one typical of carbonate ions [81], see Figure 5 and Table 5. The carbonate ions originate from the reaction of CO_2 with NaOH. The peaks at 2840 and 2490 cm^{-1} can be attributed to naphthalene ring CH stretching and also to overtones and combinations of the symmetric stretching and the out-of-plane bending of CO_3^{2-} [41,75]. The peak at 1772 cm^{-1} is an overtone of the band centred at 878 cm^{-1}, which is ascribable to CH bending of NS and to the out-of-plane bending of CO_3^{2-}. The strong peak at 1428 cm^{-1} is attributed to CH bending and CC stretching, and to -SO_2- asymmetric stretching, together with asymmetric stretching of CO_3^{2-}. Finally, the peak in the 700-665 cm^{-1} range is attributed to the skeleton distortion of NS [79]. Pristine CNTs possess conjugated carbon bonds, whose vibration modes are not detectable due to the very low concentration of CNTs in the nanofluids [73–75,82]. For all FTIR spectra, the peaks in the region between 2365-2350 cm^{-1} are attributed to atmospheric CO_2 [83].

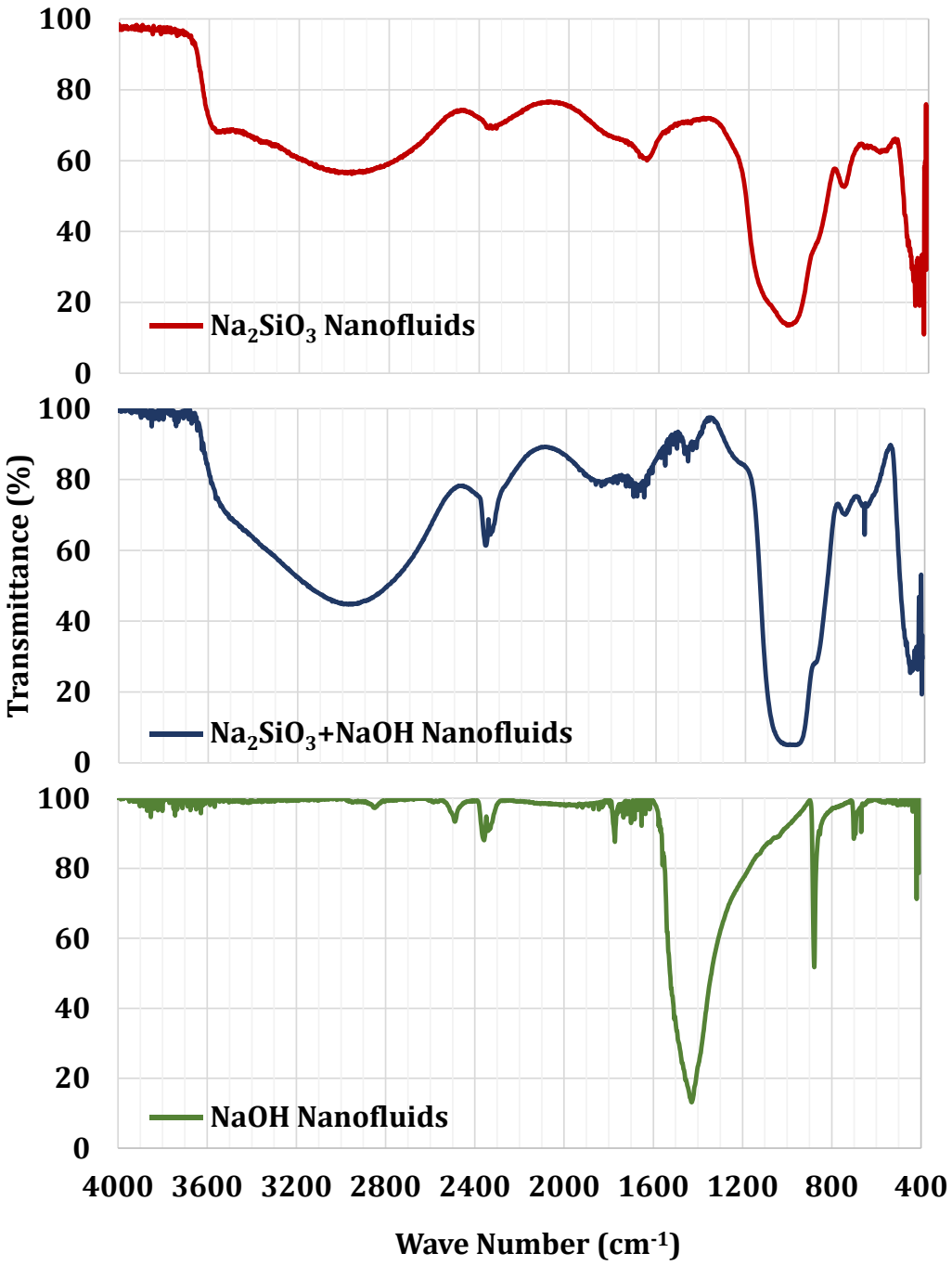

Figure 5: FTIR spectra of nanofluids.

3.1.4. Proposed dispersion mechanisms

The dispersibility and stability of MWCNTs in alkaline media and naphthalene sulfonate functionality and adsorption on MWCNTs as well have been discussed and documented in previous sections. Here, the possible mechanisms elaborated for the dispersion of MWCNTs in alkaline environments comprising Na_2SiO_3, NaOH, and combined Na_2SiO_3+NaOH will be suggested based on visual, microscopic, ILT and FTIR outputs.

Table 5: Summary of FTIR spectroscopy of nanofluids.

Methodology	**I & III**	**II**
Nanofluid / **Vibration**	Na_2SiO_3 nanofluid & Na_2SiO_3+NaOH nanofluid	NaOH nanofluid
	Frequency (cm^{-1})	
Combinations and overtones of SiO_3^{2-} species	2970	-
CH stretching of naphthalene rings		2840, 2490*
overtones of CH bending of NS	-	1772*
atmospheric CO_2	2350-2250	
symmetric & asymmetric stretching of Si-O-Si	1830 1675-1650	-
stretching of O-Si-O	1150-850	-
ring breathing of NS		
CH bending and asymmetric stretching of $–SO_2$- in NS	1457 (only Na_2SiO_3+NaOH nanofluid)	1428*
skeleton distortion of NS stretching and bending of O-Si-O	780-450	700-665 (only skeleton distortion of NS)
CH bending of NS	-	878

*these peaks are ascribable also to CO_3^{2-} vibrations

Potential physisorption

As mentioned before, MWCNTs dispersed in Na_2SiO_3 yield a uniform and stable dispersion; see ILT section 3.1.2 and Figure 4. This can be explained with the high degree of naphthalene sulfonate's physisorption on MWCNTs surface in the presence of Na_2SiO_3. This assumption is shown in Figure 6. The carbon nanotube-NS adduct is stabilized via the electrostatic interactions with Na_2SiO_3, which likely surrounds the nanotubes and minimizes the direct interaction of water molecules with the adduct. This process occurs without the competing adsorption of metasilicate ions on the surface of MWCNTs, due to the size of these poly-anions, which is relatively much larger than the adsorption sites. Moreover, the higher viscosity of Na_2SiO_3 with respect to water can decrease particle mobility and prevent NS desorption processes, via the viscous stabilization mechanism [84]; see Figure 2.

In the case of MWCNTs in NaOH and Na_2SiO_3+NaOH nanofluids, the NS-MWCNT adduct are less stable than in the presence of Na_2SiO_3 (see Figure 6). In accordance with ILT stability states in Figure 4, MWCNT desorption will take place for both NaOH and Na_2SiO_3+NaOH nanofluids. As a consequence, MWCNTs will eventually settle down in contrast to Na_2SiO_3 nanofluid, which maintain the stability of the nanocomposite for a longer time. In either of these nanofluids, OH^- ions act as competitors for the adsorption sites on the MWCNT surface [85], removing NS. This can be considered as a possible reason for the observed behaviour. This reason is theoretically elaborated in the following section. Additionally, the viscosity of the environment decreases in the presence of

NaOH, increasing the mobility of NS and favouring its desorption processes.

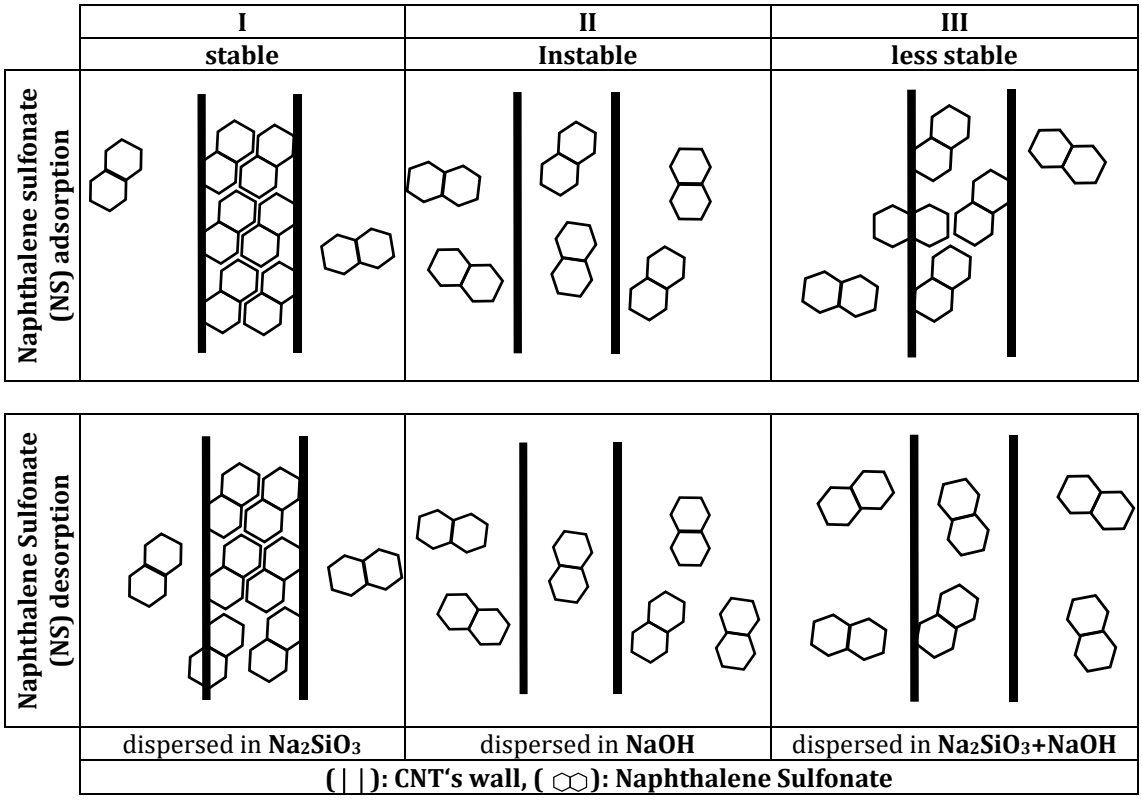

Figure 6: Stacking and physisorption of naphthalene sulfonate on MWCNTs in alkaline media; In accordance with in-solution behaviour (horizontal part of ILT graphs) of MWCNTs in alkaline media in Figure 4.

Potential electrostatic interactions

Theoretically, once the MWCNTs are dispersed in a medium with high ionic strength (e.g., NaOH), they tend to undergo agglomeration or aggregation processes, as a consequence of the electrostatic interactions of co-ions and counter-ions with the surface of the MWCNTs. The electrostatic repulsion among the MWCNTs thus fades away, inducing coalescence [86,87]. Together with the ionic strength, other physicochemical features of the dispersant medium, such as its chemical nature, viscosity, and acid-base properties, can influence the stability of the nano-system.

It can be hypothesized that OH^- ions act as competitors for the adsorption sites on carbon nanotubes [85], thus removing NS from the MWCNTs and causing instability. This does not occur in the case of metasilicate ions, due to their bigger size. In this way, the electrostatic stabilization of the nanofluid by metasilicate can be achieved without the destabilization induced by the desorption of NS from the MWCNTs. This stabilization effect is enhanced by the higher viscosity of Na_2SiO_3, in which the nanofluid has a lower diffusion coefficient [68,86]. In the case of the combined nanofluid,

394 an intermediate behaviour was observed since the concentration of OH^- ions is relatively lower than
395 in the NaOH based nanofluid.

396 **3.2. Nanocomposites' performance characterisation**

397 **3.2.1. Mechanical reinforcement**

398 According to Figure 7 and Figure 8, the dispersion characteristics of MWCNTs are clearly reflected in
399 the mechanical performance of the nanocomposites. Nanocomposites prepared by dispersing
400 MWCNTs in Na_2SiO_3 demonstrate excellent mechanical performance in both flexural and
401 compressive regimes, followed by NaOH nanocomposites. Despite that, MWCNTs incorporated by
402 dispersion in compound Na_2SiO_3+NaOH are barely capable of modifying any mechanical properties.
403 Looking back to the colloidal interactions of Na_2SiO_3 nanofluid (ref. Figure 3(b), Figure 4(b)), the
404 outstanding mechanical performance of Na_2SiO_3 nanocomposites can be ascribed to the perfect
405 dispersibility, stability, and the smallest dimension of MWCNTs within the nanofluids, all of which
406 led to an excellent in-matrix MWCNTs distribution as well.

407 Amongst the three methodologies NaOH nanocomposites show enhanced mechanical
408 performance, i.e., lower than Na_2SiO_3 but higher than compound Na_2SiO_3+NaOH nanocomposites,
409 along with mediocre colloidal behaviour; ref. Figure 3(d) and Figure 4(b). The NaOH nanofluid
410 displayed in-solution instability but long-term behaviour better than compound Na_2SiO_3+NaOH
411 nanofluid. The agglomerate dimensions were larger than those of the Na_2SiO_3 nanofluid but smaller
412 than those of the combined nanofluid. Facts as outlined led to this in-the-middle view of mechanical
413 performance in comparison to that of the other nanocomposites. Therefore, as long as the degree of
414 in-solution individualisation and in-matrix distribution reach an appropriate level, MWCNTs will be
415 capable of improving mechanical properties.

416 With respect to microscopic images and ILT measurements (ref. Figure 3(f), Figure 4(b)),
417 MWCNTs in compound Na_2SiO_3+NaOH nanofluid yielded metastable dispersion behaviour with the
418 lowest long-term stability, i.e., representative of hypothesised in-matrix behaviour, and the largest
419 agglomerate dimensions. Consequently, after MWCNTs' exposure to the alkali-activated matrix with
420 ongoing polycondensation, re-agglomeration, and cluster built-up will be easier within this
421 fabrication methodology. For this reason, MWCNTs are not that well-distributed, and many
422 concentration zones are generated throughout entire matrix. However, since the MWCNTs' mass

fraction of specimens was very small, the accumulation of agglomerates, stress concentration, and strength degradation are therefore less probable. Hence, a frequently reported structural impairment for CNT-reinforced nanocomposites, for instance in [31,38], is not found in this investigation.

When MWCNTs are dispersed in Na_2SiO_3, almost 10 MPa in 28-day flexural strength is gained which represents a reinforcement of 68% and 65% compared to the references without and with surfactant (NS), respectively. Moreover, these nanocomposites acquire compressive strength of approximately 60 MPa with 33% and 27% enhancement in comparison to the references not containing and containing NS. These nanocomposites obtain also one third of flexure and a half of compressive strengths within 3 days of matrix evolution.

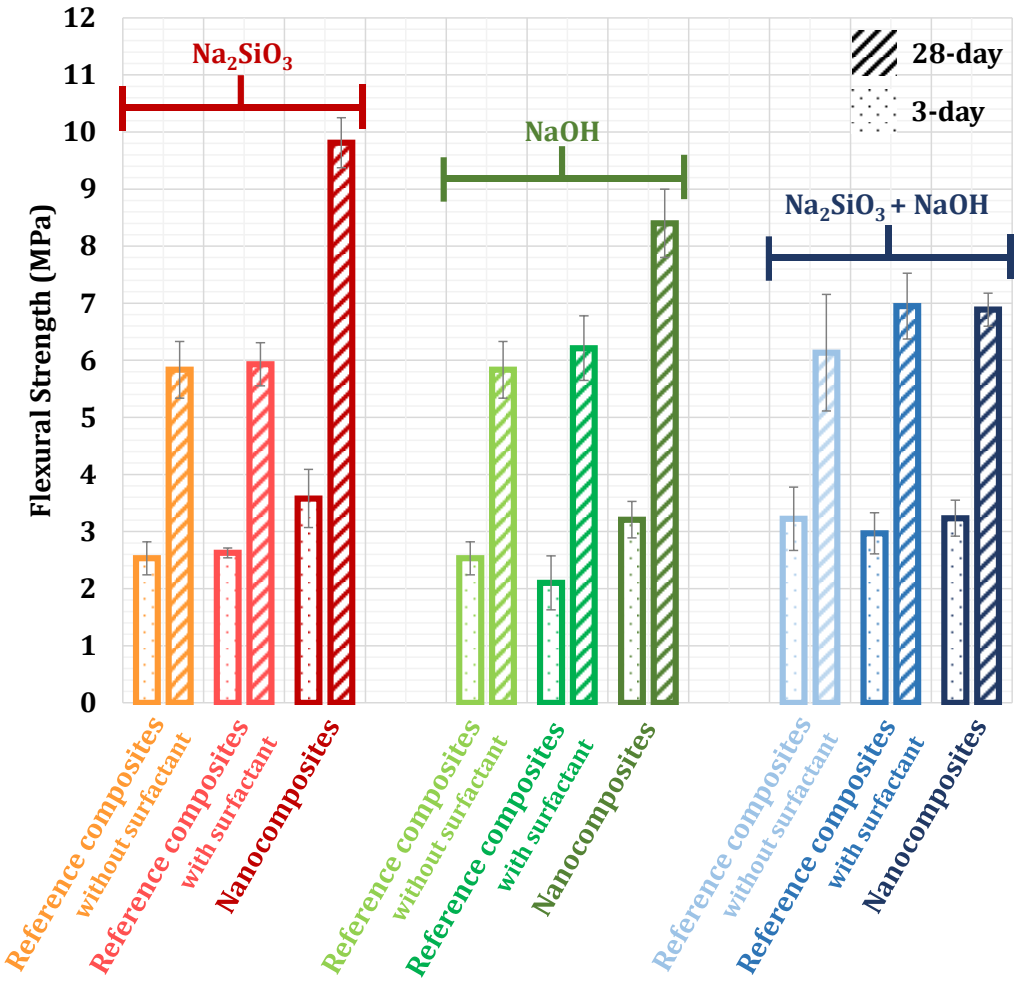

Figure 7: Mechanical performance of MWCNTs-alkali-activated-nanocomposites; Bending test; MWCNTs concentration: 0.050 wt.% of precursors in the nanocomposites.

It can be concluded that naphthalene sulfonate has imposed a slight influence on mechanical improvements of 28-day alkali-activated composites that is more for compression, 4% growth, than flexure with 2% growth in comparison to main references without NS. The positive surfactant influence on compressive strength can be better discovered for fresh 3-day specimens (Figure 8). Composites with naphthalene sulfonate inclusion have 50% higher compressive strength compared to main references without NS. This trend is valid within Na_2SiO_3 and NaOH strategies. In both strategies, MWCNTs have a negligible effect on fresh matrix strength at this age since compressive strength of nanocomposites and naphthalene sulfonate composites are approximately identical.

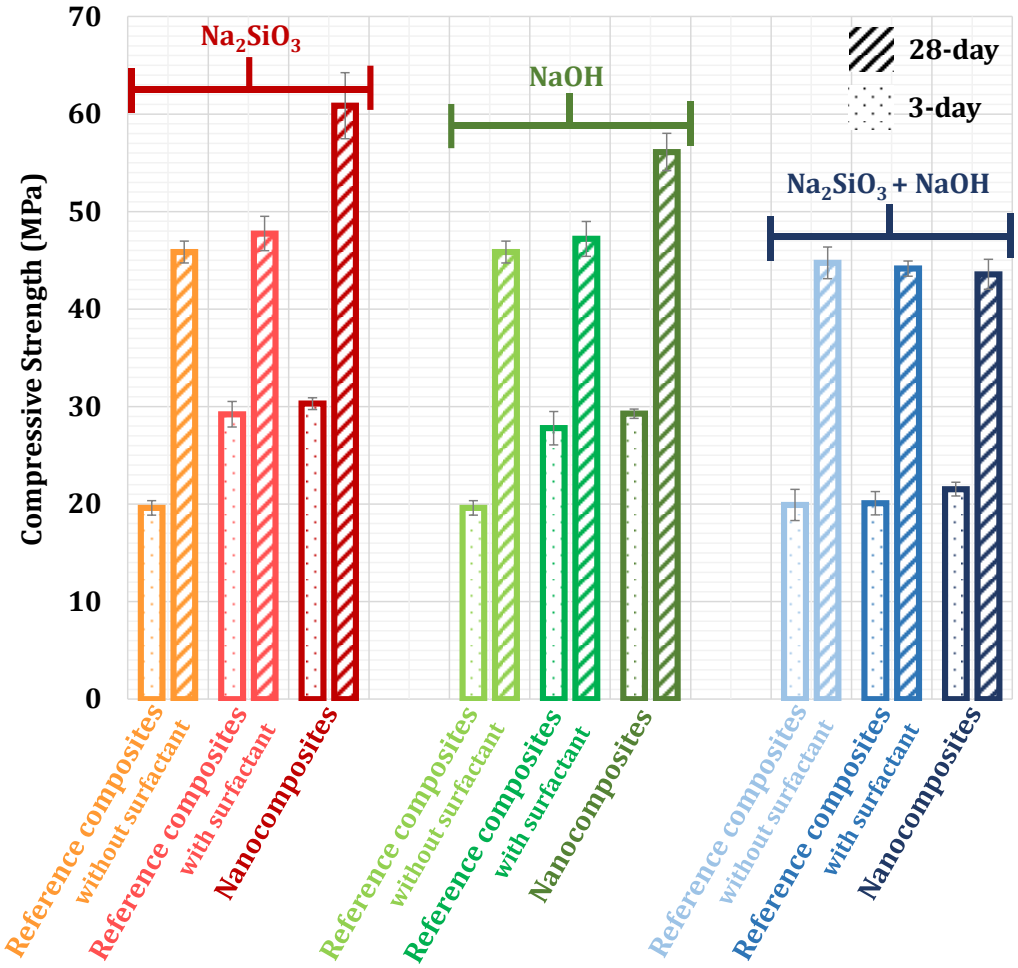

Figure 8: Mechanical performance of MWCNTs-alkali-activated-nanocomposites; Compression test; MWCNTs concentration: 0.050 wt.% of precursors in the nanocomposites.

Overall, MWCNTs' incorporation can modify flexural strength to a greater degree than compression in this FA-GGBS-alkali-activated matrix. The gain in flexural strength, that is not a case

for compression as explained above, can be even found for fresh 3-day nanocomposites. Additionally, MWCNT concentration is as low as 0.050 wt.% of solid precursors and is not functionalized, but the mechanical improvement is more pronounced than higher mass fractions and functionalised examples in MWCNTs-metakaolin-geopolymeric matrices [31] and MWCNTs-slag-alkali-activated matrices [38]. As mentioned previously, the major parameters influencing mechanical performance of nanocomposites can be dispersion quality alongside the degree of spatial distribution of CNTs throughout the entire matrix, i.e., homogeneity/heterogeneity of nanocomposite. Appropriate interfacial adhesion between CNTs and matrix is additionally amongst these factors determining to what extent CNTs' inherent potentials can be captured within the nanocomposite [88]. Considering these reasons, the aforementioned mechanical improvements can be well validated by the following microstructure including morphology and porosity study of nanocomposites.

3.2.2. Microstructure refinement

As proven before, when MWCNTs are incorporated into an alkali-activated matrix by liquid alkaline activators, the colloidal behaviour of derivative nanofluids will correspondingly control the MWCNTs' behaviour and functionality throughout the composite. Considering the nano/micro dimensions of MWCNTs, they can initially refine nano/micro texture of matrix and consequently the meso/macro structural properties of the resultant nanocomposite. Here, the microstructure has been examined by SEM and MIP measurements to figure out the reinforcement mechanisms of MWCNTs.

Morphology

Non-reinforced composites had a mechanical strength of 6 MPa and 46 MPa under bending and compression forces, respectively; see Figure 7 and Figure 8. Hence, inherently these composites have adequate integrity, compactness, and binding ability; see Figure 9. However, in addition to the aforementioned mechanisms in the paragraph above, intrinsic strength and elongation of MWCNTs along with their fibrous morphology can provide the matrix with the cohesion required for load-bearing, fracture anchorage, and the prevention of crack propagation throughout these nanocomposites, as can be clearly seen in Figure 10. Therefore, it is again evident here that pronounced enhancements of structural performance of Na_2SiO_3 nanocomposites can be attributable to highly in-solution-dispersed and in-matrix-distributed MWCNTs.

According to Figure 10(a), MWCNTs are well distributed all around the matrix in MWCNTs+NS+Na_2SiO_3 nanocomposites. The smallest agglomerate dimension within this methodology contributes the most to the availability of the largest quantity of MWCNT individuals; ref. Figure 3. Additionally, better long-term stability of MWCNTs+NS+Na_2SiO_3 nanofluids in Figure 4(b), i.e., representative of in-matrix behaviour, leads to this superior MWCNTs spatial distribution, highlighted by blue boxes, which was not observed within NaOH and Na_2SiO_3+NaOH combined strategies, i.e., the best nanocomposite homogeneity. As a result of the excellent distribution and reinforcement, the least extent and density of cracks are observed within MWCNTs+NS+Na_2SiO_3 nanocomposites. An example of the reinforcement capability of MWCNTs is illustrated in Figure 10(b), where a fracture around a small fly ash sphere is constrained and crack propagation is fully controlled by a concentration zone of MWCNTs, as highlighted by blue boxes. Adjacent supporting MWCNT clusters also contribute to this reinforcement efficiency.

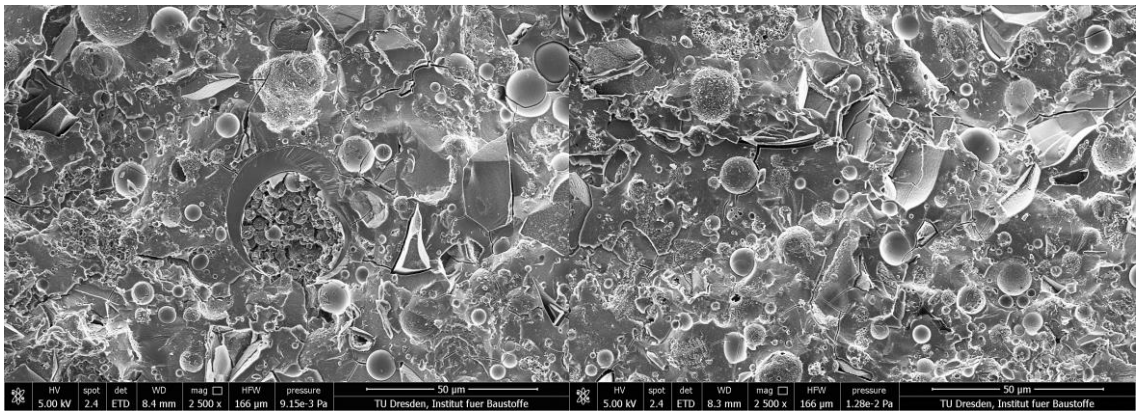

Figure 9: FA-GGBS-alkali-activated matrix; 28-day composites.

When MWCNTs are dispersed in NaOH, the spatial in-matrix distribution is observed to a lesser extent as compared to MWCNTs+NS+Na_2SiO_3 nanocomposites, consequently wider and longer cracks are detected by SEM in nanocomposites; see Figure 10(c, d). With regard to the mechanical performance of MWCNTs+NS+NaOH nanocomposites (ref. Figure 7, Figure 8), distribution of MWCNTs, highlighted by blue boxes, can be still considered within an acceptable range and perfect crack confinement and anchorage (Figure 10(c)) and coalescence control (Figure 10(d)) are observed around ruptured areas by MWCNTs throughout these nanocomposites, highlighted by blue boxes. Contrarily, in the compound MWCNTs+NS+Na_2SiO_3+NaOH methodology, ineffective MWCNTs clusters which seem incapable of matrix reinforcement are detected mostly in highly fractured zones

not distributed throughout the entire matrix; see Figure 10(e, f). MWCNTs are predominantly in de-bonded and non-load-bearing conditions, as highlighted by the red and purple boxes. Nevertheless, the aforementioned excellent elongation of MWCNTs is observed in Figure 10(e, f) for load bearing MWCNTs, highlighted by blue boxes. When there have been such large-span-micro cracks, researchers even reported CNT breakage [51], which is not the case here. Having the most long-term unstable nanofluid and containing the least quantity of dissociated MWCNTs result in this nanocomposite heterogeneity and, consequently, the largest crack widths; see ref. Figure 4 and Figure 3.

The hardening rate of nanocomposites can be another important reason. When herein the investigated alkali-activated matrix was prepared by a combined activator, i.e., Na_2SiO_3+NaOH, the observed setting time was higher than the preparation methodologies for separate activators. Therefore, there are more grounds for MWCNTs' re-agglomeration and cluster built-up in this strategy. Generally, MWCNTs share their crack-propagation-control mechanisms within different host matrices. Similarly, researchers reported MWCNTs' micro-crack-bridging in metakaolin geopolymer [31], slag alkali-activated [38], and cementitious paste [16], mortar [51], and concrete [52].

Porosity

The inclusion of MWCNTs and their incorporation methodologies influence pore distribution and dimension of 28-day nanocomposites to a great degree, as illustrated in Figure 11 and Figure 12, particularly in Na_2SiO_3 based nanocomposites. According to Figure 11(a), the cumulative pore volume of these nanocomposites reaches 99 mm^3g^{-1}, which is the smallest compared to the other nanocomposites. The most frequently detected pore dimension for Na_2SiO_3 based nanocomposites is 7 nm, located in the region of ultra-fine gel pores, i.e., D<10 nm, with the frequency in the middle; see Figure 11(b). Despite NaOH based nanocomposites' having a lower frequency in this dimension, there is another peak located at 0.45 μm in the region of capillary macro pores, i.e., 50 nm <D, observed just for these nanocomposites, i.e., containing higher amount of larger pores. The highest apex of ultra-fine gel pores, i.e., D<10 nm, belongs to the combined Na_2SiO_3+NaOH based nanocomposites, which as a consequence caused a surge of up to 110 mm^3g^{-1} in total pore volume. In Na_2SiO_3 based methodology with the dimensional transition from capillary meso-pores, i.e., D<50

nm, to capillary macro-pores, i.e., 50 nm <D, the total volume is reduced dramatically. This is a case for the combined approach as well. However, cumulative pore volume of NaOH based nanocomposites suddenly drops far beyond, at around 0.40 μm, demonstrating a diverse range of pore dimensions.

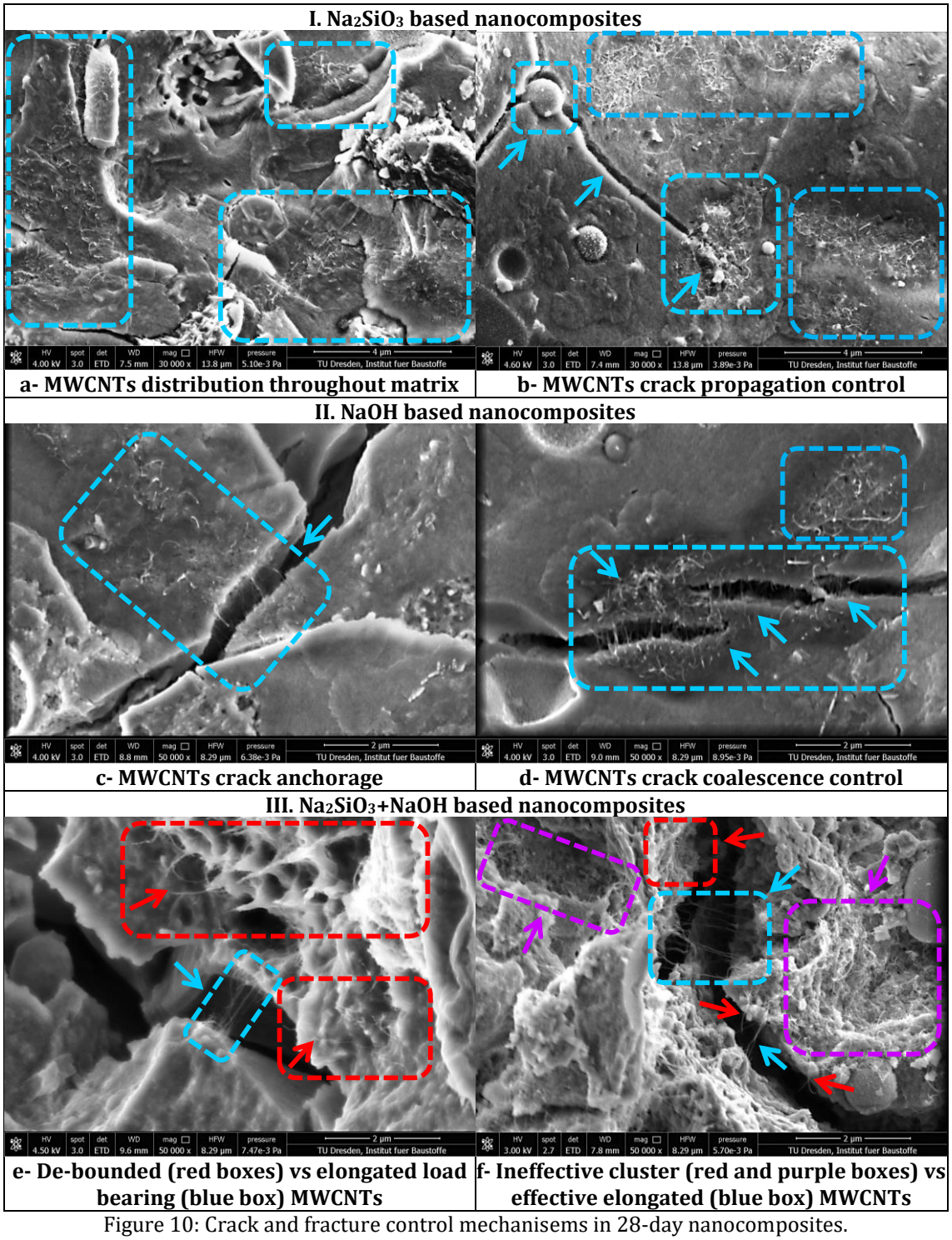

Figure 10: Crack and fracture control mechanisems in 28-day nanocomposites.

Generally, all nanocomposites have very sharp ascent in cumulative pore volumes in the region of ultra-fine gel pores, reflecting the abundance of gel pores for all strategies. On the contrary, they contain rather small quantities of super-large capillary pores, i.e., D>1 µm. The trend is valid for reference composites as well (Figure 12); therefore, it can be considered as an intrinsic property of this investigated FA-GGBS alkali-activated microstructure in comparison to [15,31,38,89].

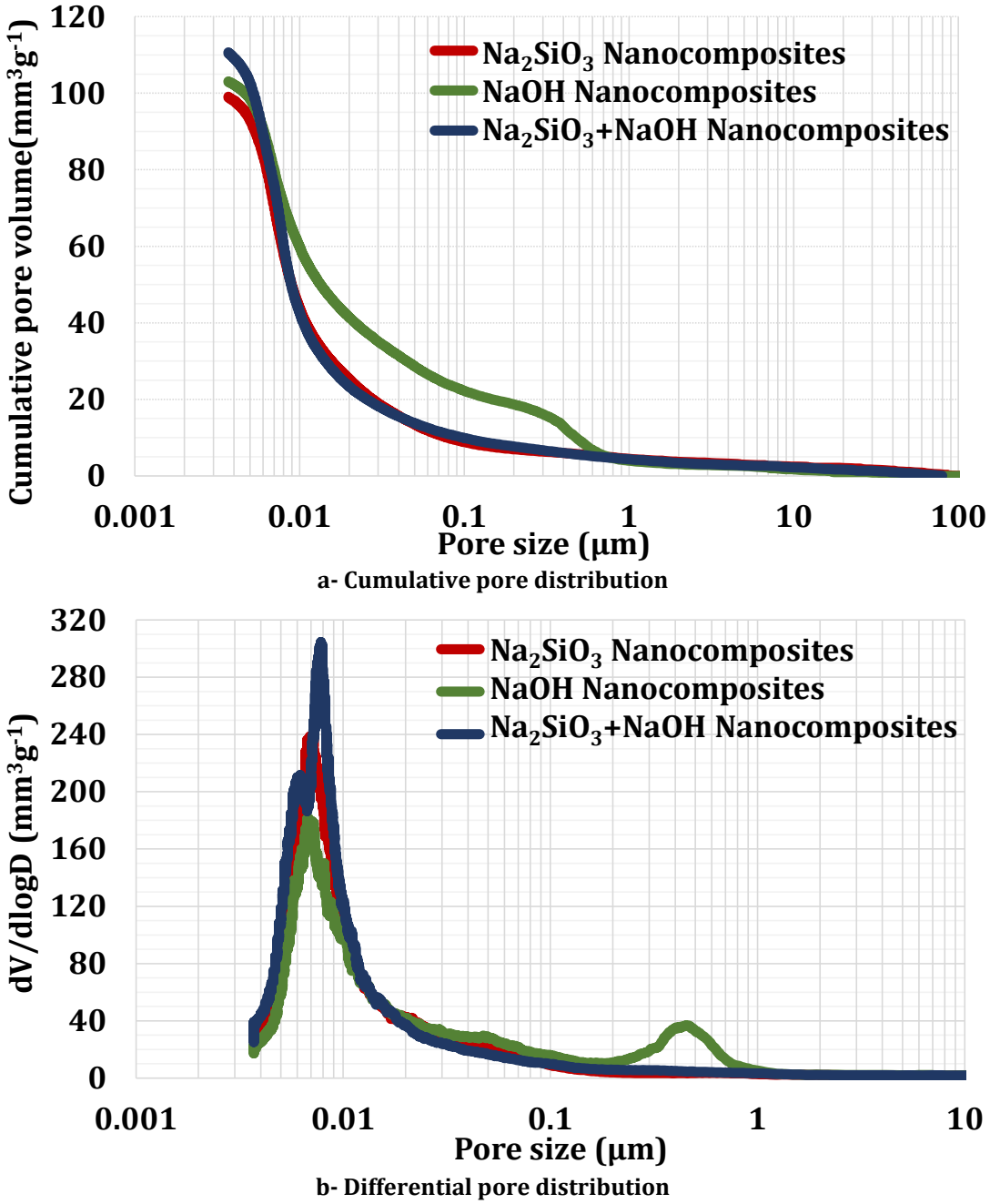

Figure 11: Pore properties of 28-day MWCNTs alkali-activated nanocomposites.

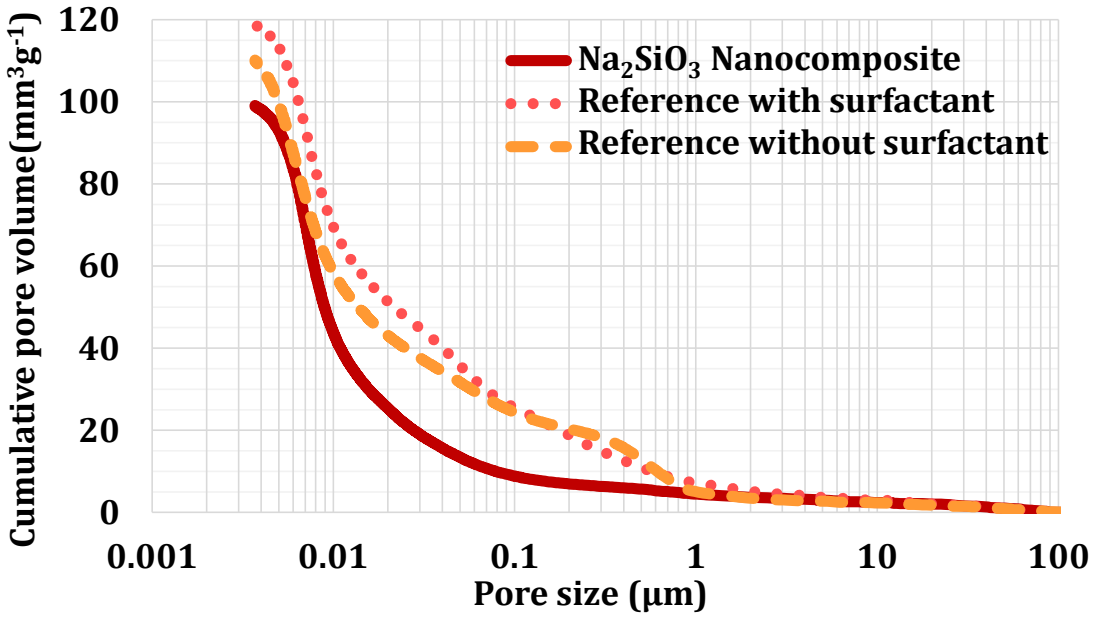

a- Cumulative pore distribution (I. Na_2SiO_3 based nanocomposites)

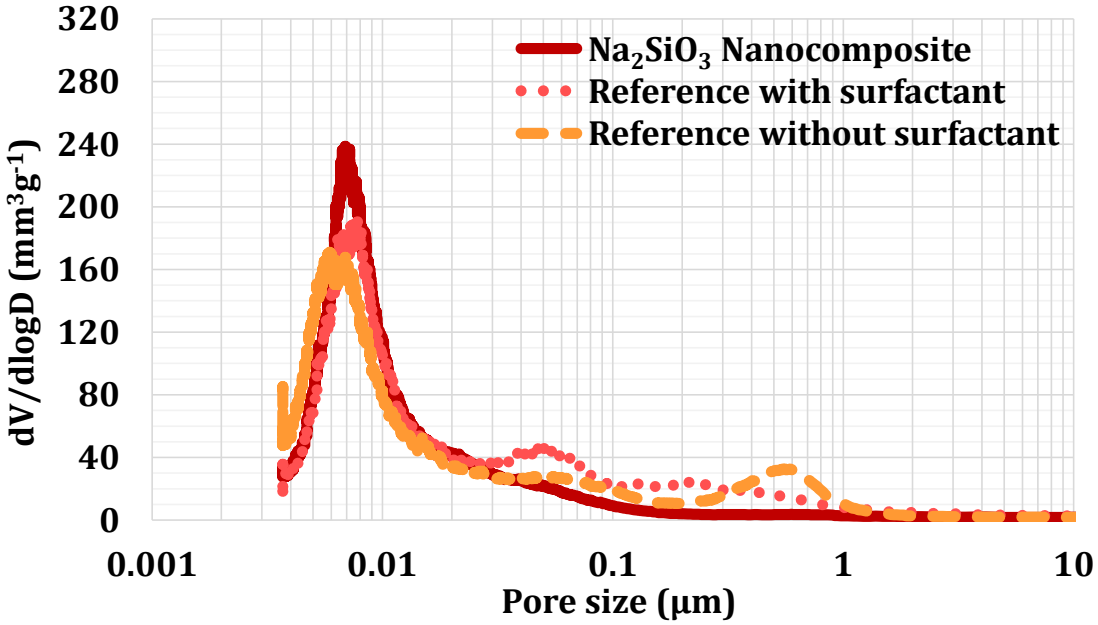

b- Differential pore distribution (I. Na_2SiO_3 based nanocomposites)

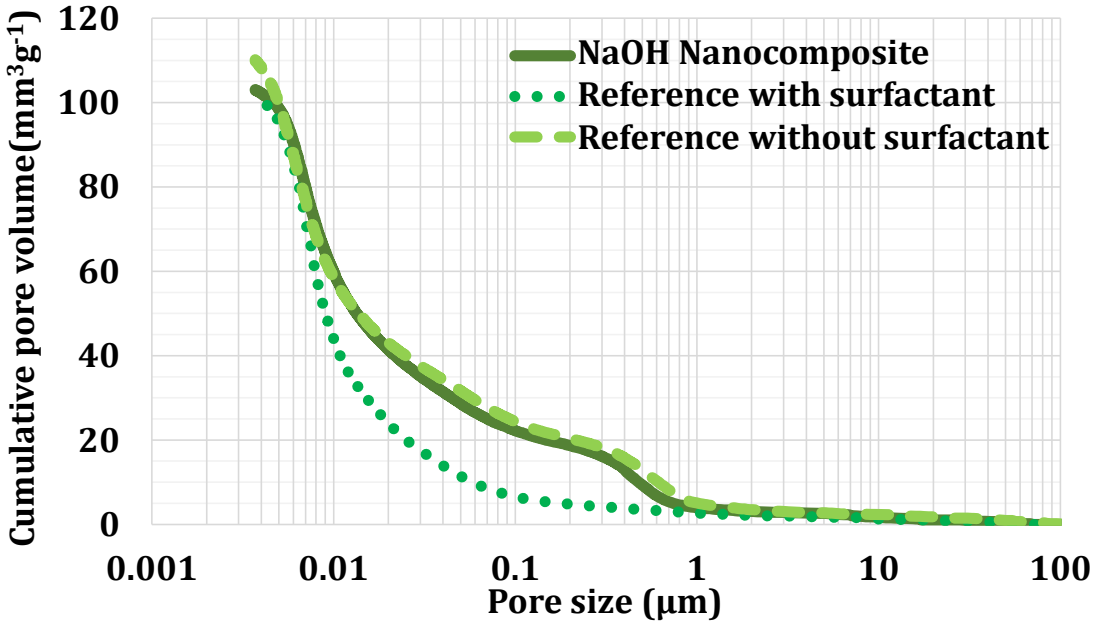

c- Cumulative pore distribution (II. NaOH based nanocomposites)

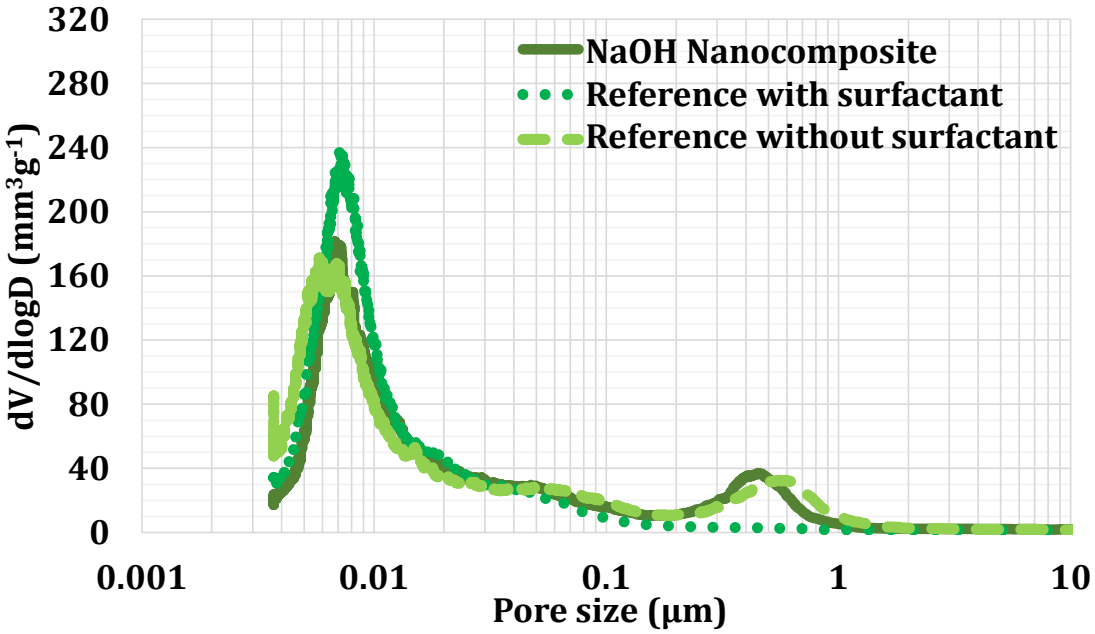

d- Differential pore distribution (II. NaOH based nanocomposites)

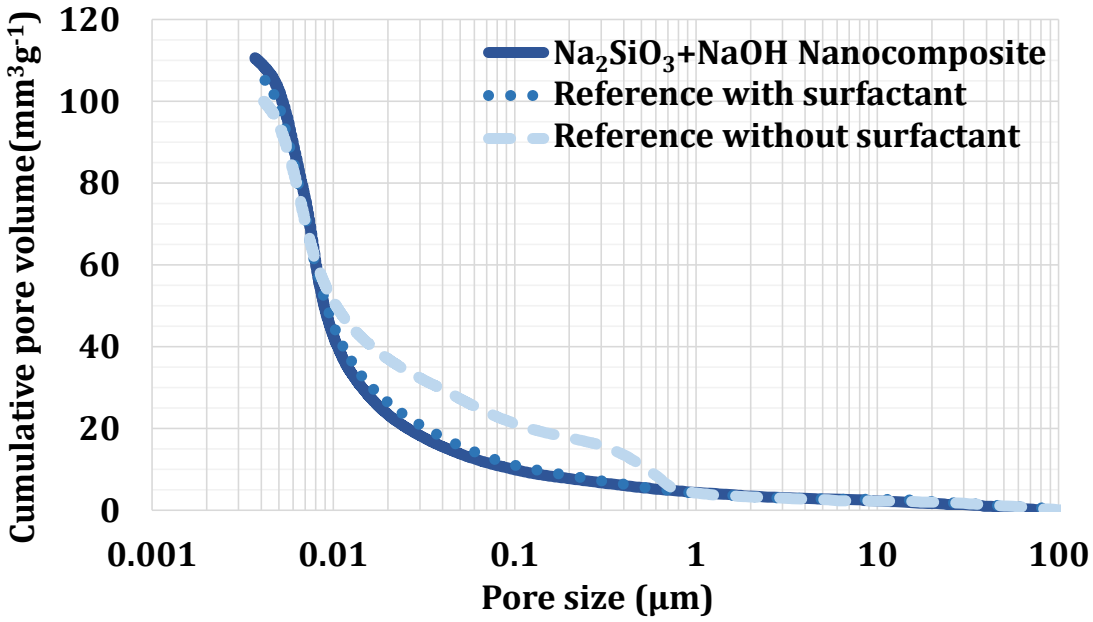

e- Cumulative pore distribution (III. Na_2SiO_3+NaOH based nanocomposites)

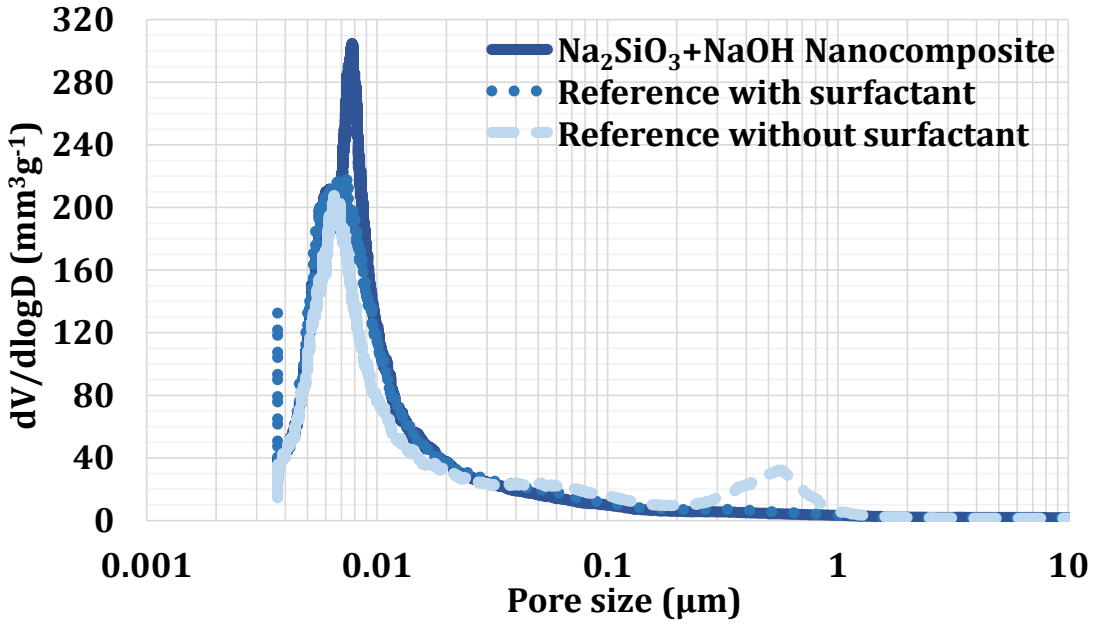

f- Differential pore distribution (III. Na_2SiO_3+NaOH based nanocomposites)

Figure 12: Pore properties of 28-day MWCNTs alkali-activated nanocomposites and composites.

In parallel, the pore refinement of MWCNTs in Na_2SiO_3 nanocomposites as mentioned is distinct in comparison to the reference composites; see Figure 12(a,b). The cumulative pore volumes of the references are much higher than those of the nanocomposites; especially naphthalene-sulfonate-included composites reach as high as 120 mm^3g^{-1}. In the transition boundary of ultra-fine gel pores, i.e., D≈10 nm, the cumulative volumes reach approximately 40, 55, and 70 mm^3g^{-1} for nanocomposites, main reference composites, and naphthalene sulfonate composites, respectively.

This probably can be interpreted as a surfactant effect which introduces air bubbles into the matrix during preparation, ultrasonication, and interaction with the precursors. In the capillary region there are two additional peaks at 54 nm and 550 nm for the main references and 47 nm and 226 nm for the naphthalene-sulfonate-containing references with wide differential distributions. Nonetheless, MWCNTs could effectively fill the pores in this dimension range, and there is no apex detectable in the relevant nanocomposites since the pores have been shifted well behind the capillary area.

The adverse naphthalene-sulfonate impact observed in the Na_2SiO_3 strategy is not detectable in the NaOH group. The largest pore volume belongs to the main reference composites without naphthalene sulfonate and the lowest belongs to the naphthalene sulfonate-composites. Unexpectedly, the capillary pore shift to the gel pore region is observed for naphthalene sulfonate-composites, not for nanocomposites. Nanocomposites and the main reference composites display rather the same microstructural features (Figure 12(c,d)).

Table 6: Advantageous decrease (negative sign) and disadvantageous increase (positive sign) in pore properties of 28-day MWCNTs alkali-activated nanocomposites compared to NS-references (containing naphthalene sulfonate) and main references.

Methodology	**I**		**II**		**III**	
Nanocomposite	Na_2SiO_3 compared to		NaOH compared to		Na_2SiO_3+NaOH compared to	
Composite / **Pore parameter**	Reference	NS-Reference	Reference	NS-Reference	Reference	NS-Reference
Average pore diameter (%)	-5	-23	+19	+28	-11	-2
Porosity (%)	-8	-14	-6	0	+6	+1
Total pore volume (%)	-10	-17	-6	+1	+8	+3
Max pore diameter (%)	+19	-10	+17	-4	+20	+5

Based on the results discussed, it can be seen that MWCNTs pre-dispersed in Na_2SiO_3, while displaying the best nanofiller dispersion and the smallest aggregate dimension, show significant pore refinement in comparison to naphthalene sulfonate included reference composites; see Table 6. Average and maximum diameters, porosity, and total volume have been enhanced herein with the best performance in average pore diameter and total pore volume, reductions of 23% and 17%, respectively. Nanocomposites of MWCNTs pre-dispersed in NaOH have conversely 28% and 2% respective increases in the mentioned parameters, reflected in the weaker mechanical properties of

574 this strategy. MWCNTs within the combined incorporation strategy do not have any significant
575 impact on the pore properties of nanocomposites; see Figure 12(e,f) and Table 6.

576 **4. Conclusions**

577 In the research presented, the fabrication of MWCNTs-FA-GGBS-alkali-activated nanocomposites has
578 been explained based on the ground of incorporating MWCNTs dispersed in three concentrated
579 alkaline activators: sodium silicate, sodium hydroxide, and combined sodium silicate and sodium
580 hydroxide. Overall, MWCNTs' incorporation into the sodium silicate strategy has demonstrated the
581 most outstanding colloidal, mechanical, and microstructural accomplishments in comparison to the
582 other incorporation methodologies. The most significant findings of this research can be summarised
583 in the following:

584 • Physicochemical properties, i.e., presence of silicon, solid concentration, and viscosity of
585 sodium silicate contribute the most to the dispersion status of MWCNTs.
586 • The smallest size of MWCNT bundles is observed in sodium silicate.
587 • MWCNTs in sodium silicate nanofluids exhibit the most stable short-term and long-term
588 behaviours.
589 • The best MWCNTs' in-matrix spatial distribution and crack propagation control have been
590 observed in sodium silicate nanocomposites.
591 • MWCNTs within sodium silicate nanofluids are capable of microstructure refinement,
592 particularly in average pore diameter, total pore volume, and porosity percentage.

593 In summary, this study can provide a great contribution to the future research and
594 development of MWCNTs alkali-activated nanocomposites with multifunctional purposes such as
595 structural health monitoring. Moreover, the obtained results build an excellent base to incorporate
596 other nanocarbon materials, such as graphene by the proposed approach or expand this knowledge
597 to one-part mixing technologies, which will be a part of a near future study.

598

References

[1] Provis JL, van Deventer JSJ. Geopolymers and Other Alkali-Activated Materials. Lea's Chem. Cem. Concr., Elsevier; 2019, p. 779–805. https://doi.org/10.1016/b978-0-08-100773-0.00016-2.

[2] Shi C, Qu B, Provis JL. Recent progress in low-carbon binders. Cem Concr Res 2019;122:227–50. https://doi.org/10.1016/J.CEMCONRES.2019.05.009.

[3] Puertas F, Torres-Carrasco M, Alonso MM.

Reuse of urban and industrial waste glass as a novel activator for alkali-activated slag cement pastes: A case study. Handb. Alkali-Activated Cem. Mortars Concr., Elsevier Inc.; 2015, p. 75–109. https://doi.org/10.1533/9781782422884.1.75.

[4] Zhang P, Zheng Y, Wang K, Zhang J. A review on properties of fresh and hardened geopolymer mortar. Compos Part B Eng 2018;152:79–95. https://doi.org/10.1016/J.COMPOSITESB.2018.06.031.

[5] Provis JL, Palomo A. Advances in understanding alkali-activated materials. Cem Concr Res 2015;78:110–25. https://doi.org/10.1016/J.CEMCONRES.2015.04.013.

[6] Zhang D, Yu J, Wu H, Jaworska B, Ellis BR, Li VC. Discontinuous micro-fibers as intrinsic reinforcement for ductile Engineered Cementitious Composites (ECC). Compos Part B Eng 2020;184:107741. https://doi.org/10.1016/J.COMPOSITESB.2020.107741.

[7] Ranjbar N, Zhang M. Fiber-reinforced geopolymer composites: A review. Cem Concr Compos 2020;107:103498. https://doi.org/10.1016/J.CEMCONCOMP.2019.103498.

[8] Guo L, Wu Y, Xu F, Song X, Ye J, Duan P, et al. Sulfate resistance of hybrid fiber reinforced metakaolin geopolymer composites. Compos Part B Eng 2020;183:107689. https://doi.org/10.1016/J.COMPOSITESB.2019.107689.

[9] Ling Y, Wang K, Li W, Shi G, Lu P. Effect of slag on the mechanical properties and bond strength of fly ash-based engineered geopolymer composites. Compos Part B Eng 2019;164:747–57. https://doi.org/10.1016/J.COMPOSITESB.2019.01.092.

[10] Constâncio Trindade AC, Curosu I, Liebscher M, Mechtcherine V, de Andrade Silva F. On the mechanical performance of K- and Na-based strain-hardening geopolymer composites (SHGC) reinforced with PVA fibers. Constr Build Mater 2020;248:118558. https://doi.org/10.1016/J.CONBUILDMAT.2020.118558.

[11] Adesina A. Performance of fibre reinforced alkali-activated composites – A review. Materialia 2020;12:100782. https://doi.org/10.1016/j.mtla.2020.100782.

[12] Farina I, Modano M, Zuccaro G, Goodall R, Colangelo F. Improving flexural strength and toughness of geopolymer mortars through additively manufactured metallic rebars. Compos Part B Eng 2018;145:155–61. https://doi.org/10.1016/j.compositesb.2018.03.017.

[13] Poletanovic B, Dragas J, Ignjatovic I, Komljenovic M, Merta I. Physical and mechanical properties of hemp fibre reinforced alkali-activated fly ash and fly ash/slag mortars. Constr Build Mater 2020;259:119677. https://doi.org/10.1016/j.conbuildmat.2020.119677.

[14] Masi G, Rickard WDA, Bignozzi MC, Van Riessen A. The effect of organic and inorganic fibres on the mechanical and thermal properties of aluminate activated geopolymers. Compos Part B Eng 2015;76:218–28. https://doi.org/10.1016/j.compositesb.2015.02.023.

[15] Carabba L, Santandrea M, Carloni C, Manzi S, Bignozzi MC. Steel fiber reinforced geopolymer matrix (S-FRGM) composites applied to reinforced concrete structures for strengthening applications: A preliminary study. Compos Part B Eng 2017;128:83–90. https://doi.org/10.1016/J.COMPOSITESB.2017.07.007.

[16] Sikora P, Abd Elrahman M, Chung S-Y, Cendrowski K, Mijowska E, Stephan D. Mechanical and microstructural properties of cement pastes containing carbon nanotubes and carbon nanotube-silica core-shell structures, exposed to elevated temperature. Cem Concr Compos 2019;95:193–204. https://doi.org/10.1016/J.CEMCONCOMP.2018.11.006.

[17] Tian Z, Li Y, Zheng J, Wang S. A state-of-the-art on self-sensing concrete: Materials, fabrication and properties. Compos Part B Eng 2019;177:107437. https://doi.org/10.1016/J.COMPOSITESB.2019.107437.

[18] Öztürk O, Yıldırım G, Keskin ÜS, Siad H, Şahmaran M. Nano-tailored multi-functional cementitious composites. Compos Part B Eng 2020;182:107670. https://doi.org/10.1016/J.COMPOSITESB.2019.107670.

[19] Paul SC, van Rooyen AS, van Zijl GPAG, Petrik LF. Properties of cement-based composites using nanoparticles: A comprehensive review. Constr Build Mater 2018;189:1019–34. https://doi.org/10.1016/J.CONBUILDMAT.2018.09.062.

[20] Singh NB, Middendorf B. Geopolymers as an alternative to Portland cement: An overview. Constr Build Mater 2020;237:117455. https://doi.org/10.1016/J.CONBUILDMAT.2019.117455.

[21] Sumesh M, Alengaram UJ, Jumaat MZ, Mo KH, Alnahhal MF. Incorporation of nano-materials in cement composite and geopolymer based paste and mortar – A review. Constr Build Mater 2017;148:62–84. https://doi.org/10.1016/J.CONBUILDMAT.2017.04.206.

[22] Gao Y, Jing HW, Chen SJ, Du MR, Chen WQ, Duan WH. Influence of ultrasonication on the dispersion and enhancing effect of graphene oxide–carbon nanotube hybrid nanoreinforcement in cementitious composite. Compos Part B Eng 2019;164:45–53. https://doi.org/10.1016/J.COMPOSITESB.2018.11.066.

[23] Longhi MA, Walkley B, Rodríguez ED, Kirchheim AP, Zhang Z, Wang H. New selective dissolution process to quantify reaction extent and product stability in metakaolin-based geopolymers. Compos Part B Eng 2019;176:107172. https://doi.org/10.1016/J.COMPOSITESB.2019.107172.

[24] Nematollahi B, Sanjayan J, Shaikh FUA. Matrix design of strain hardening fiber reinforced engineered geopolymer composite. Compos Part B Eng 2016;89:253–65. https://doi.org/10.1016/J.COMPOSITESB.2015.11.039.

[25] Liew KM, Kai MF, Zhang LW. Carbon nanotube reinforced cementitious composites: An overview. Compos Part A Appl Sci Manuf 2016;91:301–23. https://doi.org/10.1016/J.COMPOSITESA.2016.10.020.

[26] Rovnaník P, Šimonová H, Topolář L, Bayer P, Schmid P, Keršner Z. Carbon nanotube reinforced alkali-activated slag mortars. Constr Build Mater 2016;119:223–9. https://doi.org/10.1016/j.conbuildmat.2016.05.051.

[27] Khater HM, Abd el Gawaad HA. Characterization of alkali activated geopolymer mortar doped with MWCNT. Constr Build Mater 2016;102:329–37. https://doi.org/10.1016/J.CONBUILDMAT.2015.10.121.

[28] Alvi MAA, Khalifeh M, Agonafir MB. Effect of nanoparticles on properties of geopolymers designed for well cementing applications. J Pet Sci Eng 2020;191:107128. https://doi.org/10.1016/J.PETROL.2020.107128.

[29] Li F, Liu L, Yang Z, Li S. Physical and mechanical properties and micro characteristics of fly ash-based geopolymer paste incorporated with waste Granulated Blast Furnace Slag (GBFS) and functionalized Multi-Walled Carbon Nanotubes (MWCNTs). J Hazard Mater 2021;401:123339. https://doi.org/10.1016/j.jhazmat.2020.123339.

[30] Li F, Liu L, ZhemingYang, Li S. Influence of modified multi-walled carbon nanotubes on the mechanical behavior and toughening mechanism of an environmentally friendly granulated blast furnace slag-based geopolymer matrix. Ceram Int 2020. https://doi.org/10.1016/j.ceramint.2020.08.203.

[31] da Luz G, Gleize PJP, Batiston ER, Pelisser F. Effect of pristine and functionalized carbon nanotubes on microstructural, rheological, and mechanical behaviors of metakaolin-based geopolymer. Cem Concr Compos 2019;104. https://doi.org/10.1016/j.cemconcomp.2019.05.015.

[32] Luukkonen T, Abdollahnejad Z, Yliniemi J, Kinnunen P, Illikainen M. One-part alkali-activated materials: A review. Cem Concr Res 2018;103:21–34. https://doi.org/10.1016/J.CEMCONRES.2017.10.001.

[33] Abdollahnejad Z, Luukkonen T, Mastali M, Giosue C, Favoni O, Ruello ML, et al. Microstructural Analysis and Strength Development of One-Part Alkali-Activated Slag/Ceramic Binders Under Different Curing Regimes. Waste and Biomass Valorization 2020;11:3081–96. https://doi.org/10.1007/s12649-019-00626-9.

[34] Luukkonen T, Sreenivasan H, Abdollahnejad Z, Yliniemi J, Kantola A, Telkki VV, et al. Influence of sodium silicate powder silica

modulus for mechanical and chemical properties of dry-mix alkali-activated slag mortar. Constr Build Mater 2020;233:117354. https://doi.org/10.1016/j.conbuildmat.2019.117354.

[35] Liebscher M, Fuge R, Schröfl C, Lange A, Caspari A, Bellmann C, et al. Temperature- and pH-Dependent Dispersion of Highly Purified Multiwalled Carbon Nanotubes Using Polycarboxylate-Based Surfactants in Aqueous Suspension. J Phys Chem C 2017;121:16903–10. https://doi.org/10.1021/acs.jpcc.7b05534.

[36] Bogas JA, Hawreen A, Olhero S, Ferro AC, Guedes M. Selection of dispersants for stabilization of unfunctionalized carbon nanotubes in high pH aqueous suspensions: Application to cementitious matrices. Appl Surf Sci 2019;463:169–81. https://doi.org/10.1016/J.APSUSC.2018.08.196.

[37] Hou J, Du W, Zhao C, Du X, Wang Z, Li S, et al. Study on the behaviors of multi-walled carbon nanotubes modified by gemini sulfonate dispersant and their reinforced magnesium matrix composite. Mater Chem Phys 2019;229:279–85. https://doi.org/10.1016/J.MATCHEMPHYS.2019.03.028.

[38] Cui H, Luo C, Sang G, Jin Y, Dong Z, Bao X, et al. Effect of carbon nanotubes on properties of alkali activated slag – A mechanistic study. J Clean Prod 2020;245:119021. https://doi.org/10.1016/J.JCLEPRO.2019.119021.

[39] Palacios M, Houst YF, Bowen P, Puertas F. Adsorption of superplasticizer admixtures on alkali-activated slag pastes. Cem Concr Res 2009;39:670–7. https://doi.org/10.1016/j.cemconres.2009.05.005.

[40] Palacios M, Puertas F. Effect of superplasticizer and shrinkage-reducing admixtures on alkali-activated slag pastes and mortars. Cem Concr Res 2005;35:1358–67. https://doi.org/10.1016/j.cemconres.2004.10.014.

[41] Pei Z, Li L, Sun L, Zhang S, Shan X, Yang S, et al. Adsorption characteristics of 1,2,4-trichlorobenzene, 2,4,6-trichlorophenol, 2-naphthol and naphthalene on graphene and graphene oxide. Carbon N Y 2013;51:156–63. https://doi.org/10.1016/J.CARBON.2012.08.024.

[42] Kim BS, Hayes RA, Ralston J. The adsorption of anionic naphthalene derivatives at the graphite-aqueous solution interface. Carbon N Y 1995;33:25–34. https://doi.org/10.1016/0008-6223(94)00101-5.

[43] Yang X, Li J, Wen T, Ren X, Huang Y, Wang X. Adsorption of naphthalene and its derivatives on magnetic graphene composites and the mechanism investigation. Colloids Surfaces A Physicochem Eng Asp 2013;422:118–25. https://doi.org/10.1016/j.colsurfa.2012.11.063.

[44] Wang F, Haftka JJH, Sinnige TL, Hermens JLM, Chen W. Adsorption of polar, nonpolar, and substituted aromatics to colloidal graphene oxide nanoparticles. Environ Pollut 2014;186:226–33. https://doi.org/10.1016/j.envpol.2013.12.010.

[45] Ania CO, Cabal B, Pevida C, Arenillas A, Parra JB, Rubiera F, et al. Effects of activated carbon properties on the adsorption of naphthalene from aqueous solutions. Appl Surf Sci 2007;253:5741–6. https://doi.org/10.1016/j.apsusc.2006.12.036.

[46] Alzahrani AZ. First-principles study on the structural and electronic properties of graphene upon benzene and naphthalene adsorption. Appl Surf Sci 2010;257:807–10. https://doi.org/10.1016/j.apsusc.2010.07.069.

[47] Liebscher M, Lange A, Schröfl C, Fuge R, Mechtcherine V, Plank J, et al. Impact of the molecular architecture of polycarboxylate superplasticizers on the dispersion of multi-walled carbon nanotubes in aqueous phase. J Mater Sci 2017;52:2296–307. https://doi.org/10.1007/s10853-016-0522-3.

[48] Yazdi MA, Liebscher M, Hempel S, Yang J, Mechtcherine V. Correlation of microstructural and mechanical properties of geopolymers produced from fly ash and slag at room temperature. Constr Build Mater 2018;191:330–41. https://doi.org/10.1016/j.conbuildmat.2018.10.037.

[49] Cui X, Han B, Zheng Q, Yu X, Dong S, Zhang L, et al. Mechanical properties and reinforcing mechanisms of cementitious composites with different types of multiwalled carbon

nanotubes. Compos Part A Appl Sci Manuf 2017;103:131–47. https://doi.org/10.1016/j.compositesa.2017.10.001.

[50] Han B, Sun S, Ding S, Zhang L, Yu X, Ou J. Review of nanocarbon-engineered multifunctional cementitious composites. Compos Part A Appl Sci Manuf 2015;70:69–81. https://doi.org/10.1016/j.compositesa.2014.12.002.

[51] Hawreen A, Bogas JA, Dias APS. On the mechanical and shrinkage behavior of cement mortars reinforced with carbon nanotubes. Constr Build Mater 2018;168:459–70. https://doi.org/10.1016/J.CONBUILDMAT.2018.02.146.

[52] Hawreen A, Bogas JA. Creep, shrinkage and mechanical properties of concrete reinforced with different types of carbon nanotubes. Constr Build Mater 2019;198:70–81. https://doi.org/10.1016/J.CONBUILDMAT.2018.11.253.

[53] Carriço A, Bogas JA, Hawreen A, Guedes M. Durability of multi-walled carbon nanotube reinforced concrete. Constr Build Mater 2018;164:121–33. https://doi.org/10.1016/j.conbuildmat.2017.12.221.

[54] Saafi M, Andrew K, Tang PL, McGhon D, Taylor S, Rahman M, et al. Multifunctional properties of carbon nanotube/fly ash geopolymeric nanocomposites. Constr Build Mater 2013;49:46–55. https://doi.org/10.1016/j.conbuildmat.2013.08.007.

[55] Tang Z, Li W, Hu Y, Zhou JL, Tam VWY. Review on designs and properties of multifunctional alkali-activated materials (AAMs). Constr Build Mater 2019;200:474–89. https://doi.org/10.1016/j.conbuildmat.2018.12.157.

[56] Fuge R, Liebscher M, Schröfl C, Oswald S, Leonhardt A, Büchner B, et al. Fragmentation characteristics of undoped and nitrogen-doped multiwalled carbon nanotubes in aqueous dispersion in dependence on the ultrasonication parameters. Diam Relat Mater 2016;66:126–34. https://doi.org/10.1016/J.DIAMOND.2016.03.026.

[57] SEPView® Manual Version 1.239 2008.

[58] Zhang Z, Zhu Y, Zhu H, Zhang Y, Provis JL, Wang H. Effect of drying procedures on pore structure and phase evolution of alkali-activated cements. Cem Concr Compos 2019;96:194–203. https://doi.org/10.1016/J.CEMCONCOMP.2018.12.003.

[59] Tkalya EE, Ghislandi M, de With G, Koning CE. The use of surfactants for dispersing carbon nanotubes and graphene to make conductive nanocomposites. Curr Opin Colloid Interface Sci 2012;17:225–32. https://doi.org/10.1016/j.cocis.2012.03.001.

[60] Xu H, Jia W, Ren S, Wang J. Magnetically responsive multi-wall carbon nanotubes as recyclable demulsifier for oil removal from crude oil-in-water emulsion with different pH levels. Carbon N Y 2019;145:229–39. https://doi.org/10.1016/J.CARBON.2019.01.024.

[61] Vaisman L, Wagner HD, Marom G. The role of surfactants in dispersion of carbon nanotubes. Adv Colloid Interface Sci 2006;128–130:37–46. https://doi.org/10.1016/j.cis.2006.11.007.

[62] O'Dea AR, Smart RSC, Gerson AR. Molecular modelling of the adsorption of aromatic and aromatic sulfonate molecules from aqueous solutions onto graphite. Carbon N Y 1999;37:1133–42. https://doi.org/10.1016/S0008-6223(98)00305-4.

[63] Gupta VK, Kumar R, Nayak A, Saleh TA, Barakat MA. Adsorptive removal of dyes from aqueous solution onto carbon nanotubes: A review. Adv Colloid Interface Sci 2013;193–194:24–34. https://doi.org/10.1016/j.cis.2013.03.003.

[64] Engel M, Chefetz B. The missing link between carbon nanotubes, dissolved organic matter and organic pollutants. Adv Colloid Interface Sci 2019;271:101993. https://doi.org/10.1016/J.CIS.2019.101993.

[65] Detriche S, Devillers S, Seffer J-F, Nagy JB, Mekhalif Z, Delhalle J. The use of water-soluble pyrene derivatives to probe the surface of carbon nanotubes. Carbon N Y 2011;49:2935–43. https://doi.org/10.1016/J.CARBON.2011.03.002.

[66] Wang F, Ma S, Si Y, Dong L, Wang X, Yao J, et al. Interaction mechanisms of antibiotic sulfamethoxazole with various graphene-

based materials and multiwall carbon nanotubes and the effect of humic acid in water. Carbon N Y 2017;114:671–8. https://doi.org/10.1016/J.CARBON.2016.12.080.

[67] Kim BS, Hayes RA, Ralston J. The adsorption of anionic naphthalene derivatives at the graphite-aqueous solution interface. Carbon N Y 1995;33:25–34. https://doi.org/10.1016/0008-6223(94)00101-5.

[68] Lin S, Shih CJ, Sresht V, Govind Rajan A, Strano MS, Blankschtein D. Understanding the colloidal dispersion stability of 1D and 2D materials: Perspectives from molecular simulations and theoretical modeling. Adv Colloid Interface Sci 2017;244:36–53. https://doi.org/10.1016/j.cis.2016.07.007.

[69] Mishchuk NA. The model of hydrophobic attraction in the framework of classical DLVO forces. Adv Colloid Interface Sci 2011;168:149–66. https://doi.org/10.1016/j.cis.2011.06.003.

[70] Montanheiro TLDA, Cristóvan FH, Machado JPB, Tada DB, Durán N, Lemes AP. Effect of MWCNT functionalization on thermal and electrical properties of PHBV/MWCNT nanocomposites. J Mater Res 2014;30:55–65. https://doi.org/10.1557/jmr.2014.303.

[71] Coates J. Interpretation of Infrared Spectra, A Practical Approach. Encycl. Anal. Chem., Chichester, UK: John Wiley & Sons, Ltd; 2006. https://doi.org/10.1002/9780470027318.a5606.

[72] Shukla A, Bhat SD, Pillai VK. Simultaneous unzipping and sulfonation of multi-walled carbon nanotubes to sulfonated graphene nanoribbons for nanocomposite membranes in polymer electrolyte fuel cells. J Memb Sci 2016;520:657–70. https://doi.org/10.1016/J.MEMSCI.2016.08.019.

[73] Bystrzejewski M, Huczko A, Lange H, Gemming T, Büchner B, Rümmeli MH. Dispersion and diameter separation of multi-wall carbon nanotubes in aqueous solutions. J Colloid Interface Sci 2010;345:138–42. https://doi.org/10.1016/J.JCIS.2010.01.081.

[74] Marković Z, Jovanović S, Kleut D, Romčević N, Jokanović V, Trajković V, et al. Comparative study on modification of single wall carbon nanotubes by sodium dodecylbenzene sulfonate and melamine sulfonate superplasticiser. Appl Surf Sci 2009;255:6359–66. https://doi.org/10.1016/J.APSUSC.2009.02.016.

[75] Hou J, Du W, Meng F, Zhao C, Du X. Effective dispersion of multi-walled carbon nanotubes in aqueous solution using an ionic-gemini dispersant. J Colloid Interface Sci 2018;512:750–7. https://doi.org/10.1016/J.JCIS.2017.10.109.

[76] Hu H, Chen N, Wei W, Li H, Jiang Z, Xu Y, et al. The effect of solvent parameters on properties of iron-based silica binary aerogels as adsorbents. J Colloid Interface Sci 2019;549:189–200. https://doi.org/10.1016/J.JCIS.2019.04.071.

[77] Efimov AM, Pogareva VG. IR absorption spectra of vitreous silica and silicate glasses: The nature of bands in the 1300 to 5000 cm-1 region. Chem Geol 2006;229:198–217. https://doi.org/10.1016/j.chemgeo.2006.01.022.

[78] Halasz I, Agarwal M, Li R, Miller N. Vibrational spectra and dissociation of aqueous Na2SiO 3 solutions. Catal Letters 2007;117:34–42. https://doi.org/10.1007/s10562-007-9141-6.

[79] Lippincott ER, O'Reilly EJ. Vibrational spectra and assignment of naphthalene and naphthalene-d-8. J Chem Phys 1955;23:238–44. https://doi.org/10.1063/1.1741947.

[80] Robinson EA. CHARACTERISTIC VIBRATIONS OF THE SULPHURYL GROUP. Can J Chem 1961;39:247–55. https://doi.org/10.1139/v61-027.

[81] Gunasekaran S, Anbalagan G, Pandi S. Raman and infrared spectra of carbonates of calcite structure. J Raman Spectrosc 2006;37:892–9. https://doi.org/10.1002/jrs.1518.

[82] El-Desoky HS, Ghoneim MM, El-badawy FM. Carbon Nanotubes Modified Electrode for Enhanced Voltammetric Sensing of Mebeverine Hydrochloride in Formulations and Human Serum Samples. J Electrochem Soc 2017;164:B212–22. https://doi.org/10.1149/2.0941706jes.

[83] Köck EM, Kogler M, Bielz T, Klötzer B, Penner S. In situ FT-IR spectroscopic study of CO2 and CO adsorption on Y2O3, ZrO2, and yttria-stabilized ZrO 2. J Phys Chem C 2013;117:17666–73. https://doi.org/10.1021/jp405625x.

[84] Łuczak J, Paszkiewicz M, Krukowska A,

Malankowska A, Zaleska-Medynska A. Ionic liquids for nano- and microstructures preparation. Part 1: Properties and multifunctional role. Adv Colloid Interface Sci 2016;230:13–28. https://doi.org/10.1016/j.cis.2015.08.006.

[85] Grosjean B, Bocquet ML, Vuilleumier R. Versatile electrification of two-dimensional nanomaterials in water. Nat Commun 2019;10. https://doi.org/10.1038/s41467-019-09708-7.

[86] Chen Q, Xu S, Liu Q, Masliyah J, Xu Z. QCM-D study of nanoparticle interactions. Adv Colloid Interface Sci 2016;233:94–114. https://doi.org/10.1016/j.cis.2015.10.004.

[87] Clark MD, Subramanian S, Krishnamoorti R. Understanding surfactant aided aqueous dispersion of multi-walled carbon nanotubes. J Colloid Interface Sci 2011;354:144–51. https://doi.org/10.1016/J.JCIS.2010.10.027.

[88] Kai MF, Zhang LW, Liew KM. Carbon nanotube-geopolymer nanocomposites: A molecular dynamics study of the influence of interfacial chemical bonding upon the structural and mechanical properties. Carbon N Y 2020;161:772–83. https://doi.org/10.1016/j.carbon.2020.02.014.

[89] Longhi MA, Rodríguez ED, Walkley B, Zhang Z, Kirchheim AP. Metakaolin-based geopolymers: Relation between formulation, physicochemical properties and efflorescence formation. Compos Part B Eng 2020;182:107671. https://doi.org/10.1016/J.COMPOSITESB.2019.107671.